Order Number 9417516

Modal properties and spontaneous emission factor in unstable-resonator semiconductor lasers

Yao, Gang, Ph.D.

City University of New York, 1994

U·M·I
300 N. Zeeb Rd.
Ann Arbor, MI 48106

Modal Properties and Spontaneous Emission Factor in Unstable-Resonator Semiconductor Lasers

by
Gang Yao

A dissertation submitted to the Graduate Faculty in Physics in partial fulfillment of the requirements for the degree of Doctor of Philosophy, The City University of New York

1994

This manuscript has been read and accepted for the Graduate Faculty in Physics in satisfaction of the dissertation requirement for the degree of Doctor in Philosophy.

01/12/94
Date

(Chair of Examining Committee)

1/12/94
Date

(Executive Officer)

Professor Janos Bergou

Professor Mark Hillery

Professor Edward A. Whittaker

Professor Azriel Z. Genack

(Supervisory Committee)

THE CITY UNIVERSITY OF NEW YORK

Abstract

Modal Properties and Spontaneous Emission Factor in Unstable-Resonator Semiconductor Lasers

by

Gang Yao

Adviser: Professor Y.C. Chen

An experimental study has been carried out on the spectral, modal, and dynamically properties of a monolithic unstable-resonator semiconductor laser. Due to the large loss and the non-power-orthogonal nature of the transverse and longitudinal modes in the unstable resonator, the spontaneous emission factor, defined as the ratio of the power of the spontaneous emission entering the lasing mode to the total power of the spontaneous emission, is much larger than that of a regular Fabry-Perot cavity of the same dimension. The large spontaneous emission factor has profound effects on the lasing properties. For a 100-μm-wide and 500-μm-long stripe-geometry unstable resonator with a convex mirror of 2.2-mm radius of curvature, the enhancement factor is measured to be 500. The large spontaneous emission factor results in a less well-defined lasing threshold, multi-longitudinal mode operation above the threshold, and strongly damped relaxation oscillation. In addition, the unstable-resonator is sensitive to the thermal lensing effect that normally occurs when the laser in under CW pumping. In the laser device used in this study, the thermal lensing effects can make the resonator more "stable", resulting in a drastic reduction in the spontaneous emission factor and nearly single longitudinal mode operation. A numerical modeling for the eigenmodes of unstable-resonator semiconductor laser with a lateral gain guiding is carried out using the wave-propagation method. The

result of numerical calculation is consistent with the experimental observations. The calculation also provides a general description of the relationship between the spontaneous emission enhancement factor and the cavity parameters such as, cavity round-trip diffraction loss, the cavity length, strip-width and the radius of curvature of the end-mirror.

To my beloved wife, Dora Nineth
for her patience, understanding and support...

Acknowledgment

Special thanks to Prof. Y. C. Chen, my dissertation supervisor, for his generous support and guidance through all these years toward the completion of this thesis. Thanks to Prof. M. Hillary and Prof. J. Bergou for their assistance in my academic study. Thanks to Prof. E. A. Whittaker and Prof. A. Z. Genack for participating in my thesis as committee members.

Table of Contents

List of Tables

List of Figures

1. Introduction

In semiconductor lasers, high-power operation in a single-spatial mode still remains to be a technological challenge because it is difficult to ensure single-mode and the large gain volume simultaneously with regular Fabry-Perot resonator. Various mode-control methods, such as laser array for example, have been developed to ensure high-power and single-spatial-mode lasing. The unstable geometrical configuration of resonator is one of commonly used approaches for such purpose. This is mainly attributed to the reason that an unstable cavity supports a fundamental spatial mode with a larger cross sectional area while effectively suppressing the higher-order spatial modes.

Previously, the properties of unstable-resonator semiconductor lasers has been studied by several groups[1-6]. Single-spatial-mode, nearly diffraction-limited operation with a several hundreds mW output has been reported [5-6]. Most of the studies on the unstable-cavity semiconductor lasers have focused on the device fabrication, lateral mode control and high output power operation.

The unstable resonator laser belongs to the class of laser cavities that may possess the non-power-orthogonality in the transverse modes and longitudinal modes. A major consequence of this non-power-orthogonality is the excess spontaneous emission factor. The spontaneous emission factor, defined as the ratio of the spontaneous-emission power entering the lasing mode to the total power of spontaneous-emission, plays an important role in determining the line-width, lasing spectrum, and the dynamic properties of the lasers with small gain-volume, such as semiconductor lasers being one example.

Recently, the excess spontaneous emission factor in unstable-cavity lasers has attracted considerable theoretical interest [8-15]. Since the time when it was first introduced in

gain-guide semiconductor lasers by Petermann [7], the excess spontaneous emission factor has been analyzed extensively for its causes and theoretical implication. According to the conventional laser theory, the spontaneous emission factor can be understood in the form of the one-photon theorem [13, 16] which states that the spontaneous-emission power entering one lasing mode is equal to the stimulation-emission power of that mode with one photon in the cavity with other conditions unchanged. The eigen mode of a resonator with a larger cross-section area is more "collimated" and, therefor, collects less spontaneous emission, which radiates in 4π solid angle. Thus, the spontaneous emission factor of a laser is inversely proportional to the cross-section area. The amount of spontaneous emission is also proportional to the bandwidth of the longitudinal modes, which, in turn, is inversely proportional to the length of the cavity. Combining these geometrical factors, the spontaneous emission factor is inversely proportional to the volume of the resonator. In general, the spontaneous emission factor can be written as:

$$\beta_0 = \lambda^4/(4\pi^2 V_{eff} \Delta\lambda_{sp} n^3)$$

where V_{eff} is the effective gain volume, $\Delta\lambda_{sp}$ is the spectral width of spontaneous emission of the gain medium and n is refractive index of the material. For a semiconductor laser with a 5 μm strip width and 200 μm length, this spontaneous emission factor is typically in the order of 10^{-6}. For a Nd:YAG laser with a gain volume of $(1\times10^{-3}\,\mathrm{m})^2 \times \pi \times 0.1\mathrm{m}$, λ=1.06 μm, $\Delta\lambda_{sp}$=6.7 Å and n=1.8, the value of β_0 is 2.6×10^{-22}.

Petermann [7] has pointed out that, in the gain-guided semiconductor lasers, the spontaneous emission factor can be enhanced by a factor of $K_p > 1$ comparing to that predicted by the one-photon theorem. In the gain-guided semiconductor lasers with a strip width of several micrometers, the enhancement factor K_p ranges from 4~10 [7]. Petermann's theory on the spontaneous emission enhancement factor has stimulated a

series of studies [10-16] on the theoretical implication of this phenomenon which seems to contradict the standard quantum laser theorem. Earlier understanding of Petermann's factor is based on the argument [8-10] that, in a gain-guided semiconductor laser resonator, the mode of the resonator has a curved wave front due to the non-uniform gain distribution in the lateral direction. The curved wave front makes these gain-guided resonator modes "improper modes" and leads to the enhancement in the spontaneous emission factor. The modes are "improper" in the sense that they no longer form a complete set of orthogonal bases. In order to describe the laser field in such resonator, these "improper mode" must be expanded in terms of a complete set of orthogonal "proper modes" of the classical one-photon theory. Thus, the spontaneous emission power entering one of these 'improper modes', determined by the expansion coefficients, is usually larger than the power into each "proper mode". An intuitive physical picture of these improper modes can be understood by thinking that a curved wave-front mode will possess more k_x components than a plane wave front so the mode collects more spontaneous emission power which is emitted randomly with 4π solid angle.

Recently, the concept of the spontaneous-emission enhancement factor has been generalized to include the effect of cavity's loss and geometrical factors such as the unstable or stable configuration[13]. According to his theory, the enhancement of the spontaneous emission power entering the lasing mode originates from the non-Hermitian property of the system operator which governs the behavior of laser resonator modes. This non-Hermitian property of resonator operator can be the results of any one of the following matters: geometrical structure of the resonator, wave-guiding mechanism of the resonator mode, and the output coupling of the resonator. One of the consequences of the non-Hermitian property of the system operator is the non-power-orthogonality of resonator's eigen-modes. If these non-power-orthogonal modes are used to expand the lasing field of the resonator, the spontaneous emission power entering these modes can be

enhanced by a factor that is larger than one. Thus, the spontaneous emission enhancement factor exists for any kind of open-ended (especially for high mirror loss) resonator and for any resonator with a set of non-power-orthogonal transverse modes. According to [13], the spontaneous emission enhancement factor K_{qn} can be expressed as:

$$K_{qn} = K_T^n \times K_L^n \tag{1}$$

where the K_T^n and K_L^n are the longitudinal and transverse enhancement factors given by

$$K_L^n = \frac{1}{|\gamma_n|^2}\left[\frac{1-|\gamma_n|^2}{2\alpha L_z}\right]^2 \tag{2}$$

$$K_T^n = \frac{\int |u_n(\bar{s})|^2 d\bar{s}}{\left|\int u_n^2(\bar{s}) d\bar{s}\right|^2} \tag{3}$$

where the n and q represent the indices of the longitudinal and transverse modes, γ_n is round trip loss of mode $u_n(\bar{s})$, α is the gain of the laser material and L_z is cavity length. The non-uniform loss and gain distribution along the longitudinal direction of the resonator (i.e. the end mirror loss) results in the enhancement factor $K_L^n > 1$. On the other hand, the biorthogonality of transverse modes results in $K_T^n > 1$. Comparing to the conventional laser rate equations, the spontaneous emission power into the lasing mode is now multiplied by a factor K_{qn} .

Thus, for an optical resonator with a set of non-power-orthogonal eigen-modes, the spontaneous-emission-power entering a lasing mode will be enhanced by a factor larger than 1 comparing to that of a set of orthogonal modes, i.e. if the β_0 is the spontaneous

emission factor for the "proper mode" then $\beta=K\beta_0$ is for the "improper mode" . The enhancement is not necessarily always caused by the curved wave front of the laser modes. For certain laser cavities, such as the stable cavities of gas and solid-state lasers with small mirror loss and the cavities of the index-guided semiconductor lasers, the resonator modes can be approximated by a set of power orthogonal modes and the Petermann's factor is very close to unit. However for laser resonators with non-power-orthogonal modes, the Petermann's factor may be substantially larger than one. Examples of such systems include the unstable laser cavities, gain or loss guided amplifiers and resonators, and variable-reflectivity-mirror lasers [11-13].

Although the theory of Petermann's enhancement factor for the unstable resonator has been widely discussed [10-16], there has been no report of experimental studies of the generalized theory of excess spontaneous emission factor. In an unstable resonator semiconductor laser, the properties of the lasing mode can be further affected by the effect of lateral gain guiding, and the analysis requires numerical method. Recently, we have carried out a study on the spontaneous emission factor in an unstable-resonator semiconductor laser. The results of the experimental and the numerical modeling show that the spontaneous emission in an unstable resonator is enhanced by two-orders of magnitude comparing to that expected in a Fabry-Perot resonator of comparable dimensions. We have found that the enhanced spontaneous emission factor results in a less pronounced threshold behavior, a broader spectral width, and quickly damped relaxation oscillations. We have also found that this enhancement of spontaneous emission can be drastically affected by the development of thermal wave guiding in the gain medium.

In this thesis, we will first, in Section II, give a brief discussion and review of the generalized theory of spontaneous emission factor based on references [13] and [14]. The

theory gives a general derivation of the relation between the cavity's guiding mechanism and the SEF. In Section III, we report the experimental investigation of the spontaneous emission factor in an unstable-resonator semiconductor laser when the laser is operating under various conditions. The general features of the laser and their relations with the system's large spontaneous emission factor due to its unstable geometric configuration are also discussed. The experimental results are compared with the numerical simulations in the Section V. Finally, a numerical modeling of the laser system in the presence of both geometric unstable resonator and lateral gain guiding mechanisms are carried out in Section IV. The numerical results are compared with the experiment data and provides a general and quantitative relation between the spontaneous emission factor and the cavity parameters.

II. Theoretical Background

In order to understand how the amount of the spontaneous emission power entering the lasing mode is affected by the wave guiding and geometrical factors of a resonator, it is useful to have a detailed study of the resonator-mode problems starting form the basic Maxwell equations. The accurate evaluation of spontaneous emission enhancement factor or SEEF., as will be seen in later part of this section, is based on the full information of the resonator modes. Various ways of solving the modal problem have been developed in the past. Two major methods used in studying the unstable resonator modes are the "geometrical method" and the "diffraction wave optics method". The geometrical method, first developed by Siegman [16], is attractive for its simplicity and straight forward ways of unveiling some important properties about the cavity modes. This method is especially useful for establishing the orders-of-magnitude estimate of modal loss and for developing an intuitive picture of the unstable resonator. On the other hand, the diffraction wave-optics method must be used for more accurate description of the laser modes. Based on

Huygens' principle, the diffraction-wave-optics methods are, in most cases, numerical modeling and calculation. The Fox-Li modes [17, 18] of resonators are examples of this method. For semiconductor lasers, the dimension of the laser resonator is between the diffraction and geometric ranges. Thus, we have adopted both methods, depending on the convenience or necessity.

II-1) Unstable Cavity: Geometrical Treatment

By the geometrical method, an unstable resonator can be defined as one with around-trip cavity magnification larger than one. With R_1 and R_2 as the radius curvatures of the two end mirrors and L as cavity length, as shown by the Figure 1, the mathematical expression for qualification of unstable resonator is:

$g_1g_2 > 1$ or $g_1g_2 < 0$ where $g_1 = (1 - L/R_1)$ and $g_2 = (1 - L/R_2)$

Physically, this means that the geometrical size of the traveling wave front of the resonator modes will be enlarged after each round trip by a factor of M, the magnification of the unstable cavity which can be expressed as:

$$M = \frac{(1+d_1)(1+d_1)}{d_1 d_2} \tag{4}$$

Where the d_1 and d_2 are the locations of two virtual sources, measured relative to the end mirrors M_1 and M_2 of the resonator. The location d_1 and d_2 of virtual source can be determined by:

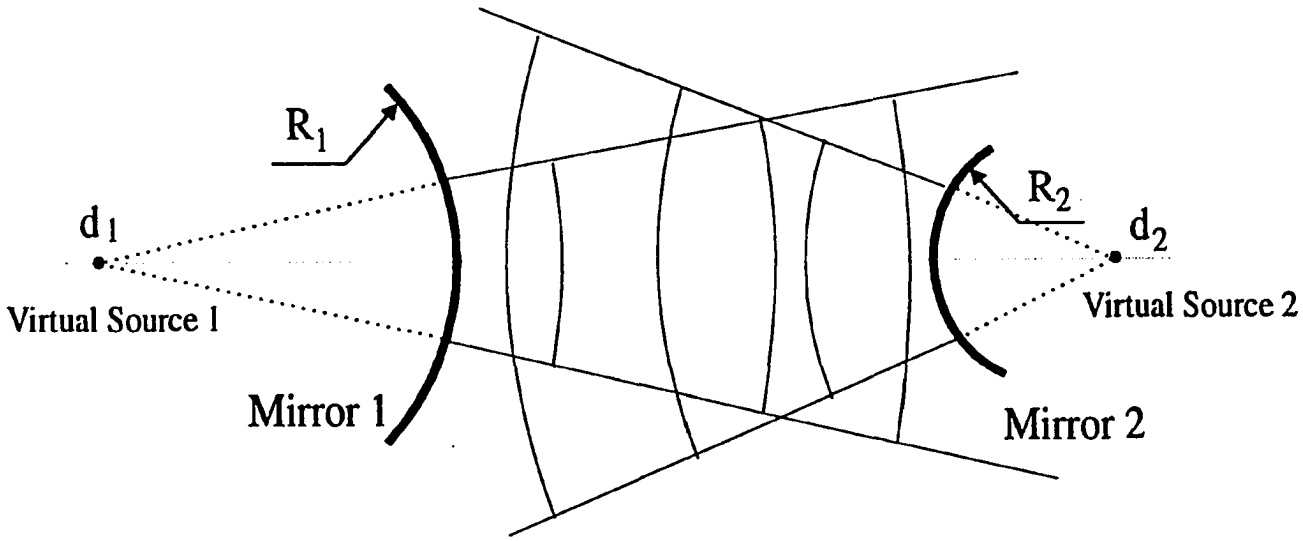

Figure 1. An unstable resonator. R_1 and R_2 are the radius of curvature of the end mirrors. L is the separation of mirrors. The locations of modal virtual sources are located at d_1 and d_2 behind the mirrors.

$$d_{1,2} = \frac{+\sqrt{1-h_1h_2} - (1-h_{1,2})}{(1-h_1)+(1-h_2)} \qquad \text{with } h_{1,2} = g_{1,2}^{-1} \tag{5}$$

With this approach, the resonator's optical mode will have a curved wave-front (which is nearly spherical) due to the finite distance location of the two virtual sources. The enlargement of the beam contributes to additional cavity loss, which we refer to as diffraction loss of the cavity. The relation between the magnification factor and the diffraction loss is $1-|\gamma|^2 = 1/\sqrt{M}$, where the γ is the fraction of field remaining inside the cavity after each round trip. For an unstable resonator, the diffraction loss is much high than the mirror reflectivity loss, and is often used as the laser output directly. The large cavity loss of unstable-cavity laser is one of the key factor that contributes to the enhancement of the spontaneous emission factor in the lasing mode.

II-2) Orthogonality of Resonator Modes

In following sections, the orthogonality of the resonator modes and its relation with the spontaneous-emission enhancement factor will be discussed following the treatment of Siegman [13].

The electric field inside a laser resonator can be described by the following scalar equation derived from Maxwell equations:

$$\nabla^2 E(\bar{r},t) - \mu\sigma \frac{\partial E(\bar{r},t)}{\partial t} - \mu\varepsilon \frac{\partial^2 E(\bar{r},t)}{\partial t^2} = \mu \frac{\partial^2 P(\bar{r},t)}{\partial t^2} \tag{6}$$

where:

μ and ε = the magnetic and dielectric permeability

$\bar{r}$ and t = space and time coordinates

σ = conductivity, representing the stimulated emission

$E(\vec{r},t)$ = electric field

$P(\vec{r},t)$ = random-noise polarization, representing the spontaneous emission

$E(\vec{r},t)$ and $P(\vec{r},t)$ can be further written as the product of a slowing varying (comparing to optical oscillation) envelop and a propagation term:

$$E(\vec{r},t) = \mathrm{Re}\left[E(\vec{r},t)e^{i(\omega t-\beta z)}\right]$$
$$P(\vec{r},t) = \mathrm{Re}\left[P(\vec{r},t)e^{i(\omega t-\beta z)}\right]$$

By using the slowly-varying-envelope approximation, we have the following equation that governs the temporal and spatial development of the slow-varying envelop of phase and amplitude of the electric field:

$$\left\{\nabla_T^2 - 2i\beta\left[\frac{\partial}{\partial z} - \alpha + \frac{1}{c}\frac{\partial}{\partial t}\right]\right\}E(\vec{r},t) = -\omega_\mu^2 P(\vec{r},t) \qquad (7)$$

Here the coordinates are chosen so that the z represents the direction of propagation of the traveling field along the resonator axis and x, y, (or $\vec{s}$=(x, y) in short), represent the transverse directions of the resonator (perpendicular to the resonator axis). In Eq. (7), ∇_T^2 is the Laplacian operator with respect to the transverse coordinates (x, y), and $\alpha=-\eta_0\sigma/2$ is the gain coefficient in the atomic medium, with $\eta_0=(\mu/\varepsilon)^{1/2}$.

The transverse eigenmodes $\{u_n(\vec{s},z)\}$ of a given resonator is a set of spatial patterns which are the solutions of the following equations with all the boundary conditions imposed by the cavity (including the effects of end mirrors) in the absence of the spontaneous emission noise term:

$$\left\{\nabla_T^2 - 2i\beta_n\left[\frac{\partial}{\partial z} - \alpha(\bar{s})\right]\right\}u_n(\bar{s},t) = 0 \tag{8}$$

Note that, equation (8) contains a spatially-distributed gain coefficient $\alpha(\bar{s})$ so that the situations considered here include those resonator modes which are guided by the gain or loss, i.e. active-wave-guiding. If the waveguide is formed by the is formed by the steps of the real part of the refractive index, the cavity modes satisfy Eq. (8) without the term $\alpha(\bar{s})$. The eigenvalue problem (8) for cavity modes can be written, in general, as :

$$\bar{\xi}(\bar{s},z,\nabla)u_n(\bar{s},z) = \gamma_n u_n(\bar{s},z) \tag{9}$$

where the system operator $\bar{\xi}$ contains all the propagation and the boundary effects of the resonator and γ_n is the eigenvalue of $u_n(\bar{s},z)$.

To understand the physical meanings of $u_n(\bar{s},z)$ and γ_n, an alternative way of expressing the eigen-value problem (9) in its integral form is often used.

For a given resonator, if an arbitrary transverse pattern of the electric field is lunched along the resonator's axis (i.e. z direction) at an arbitrary plane, the field pattern at the other plane after traveling distance L can be calculated by using Huygens principle:

$$E_2(\bar{s}_2,z_2) = \int E_1(\bar{s}_1,z_1)\times K(z_2,z_1,\bar{s}_2,\bar{s}_1)\times d\bar{s}_1 \tag{10}$$

where the integral kernel $K(z_2,z_1,\bar{s}_2,\bar{s}_1)$has all the optical components (include transverse optical gain or loss effects) of the resonator between the z_1 and z_2 . In free space, for example, the kernel K is simply:

$$K = \frac{e^{ik|\vec{s}_2 - \vec{s}_1|}}{|\vec{s}_2 - \vec{s}_1|}\cos(\theta)\ ,\ \theta = (d\vec{s}_1, \vec{s}_2 - \vec{s}) \tag{11}$$

To consider the effects of the end mirrors (i.e. when the distance between the z_1 and z_2 is large than the cavity length), the cavity can be unfolded, for convenience, into an infinitely long wave guide that is composed of equivalent lens and has a spatial period equal to the round trip length of the resonator. This idea is graphically illustrated in Figure 2.

In the lens-guide representation, the resonator loss due to both diffraction and end mirrors' reflectivity can be represented the effect of an absorption wall. The advantage of the lens-guide representation is that equation (10), which keeps track of the propagation of the wave back and forth inside the resonator, is now becoming an one-way integration along the guide. An optical mode u_n in this lens guide is such a field pattern that, if we take the distance between z_1 and z_2 to be the round trip p = 2L of the resonator (i.e. z_2=z_1 + p), the field will recover its spatial distribution in both amplitude and phase after interacting with the propagation kernel $K(z_2, z_1, \vec{s}_2, \vec{s}_1)$, i.e.:

$$\begin{aligned} &u_n(z_2 = z_1 + p, \vec{s}_2) = \int u_n(z_1, \vec{s}_1) \times K(z_1, z_2, \vec{s}_1, \vec{s}_2) d\vec{s} \\ &u_n(z_2 = z_1 + p, \vec{s}_2) = \gamma_n u_n(z_1, \vec{s}_1) \\ &\qquad\qquad \text{or} \\ &\gamma_n u_n(z_1, \vec{s}) = \int u_n(z, \vec{s}') \times K_{round-trip}(\vec{s}, \vec{s}') d\vec{s}' \end{aligned} \tag{12}$$

Physically, γ_n is the amplitude reduction and the constant phase shift of the mode u_n after an round trip. Equation (12) is just the integral form of the eigen-value problem (9).

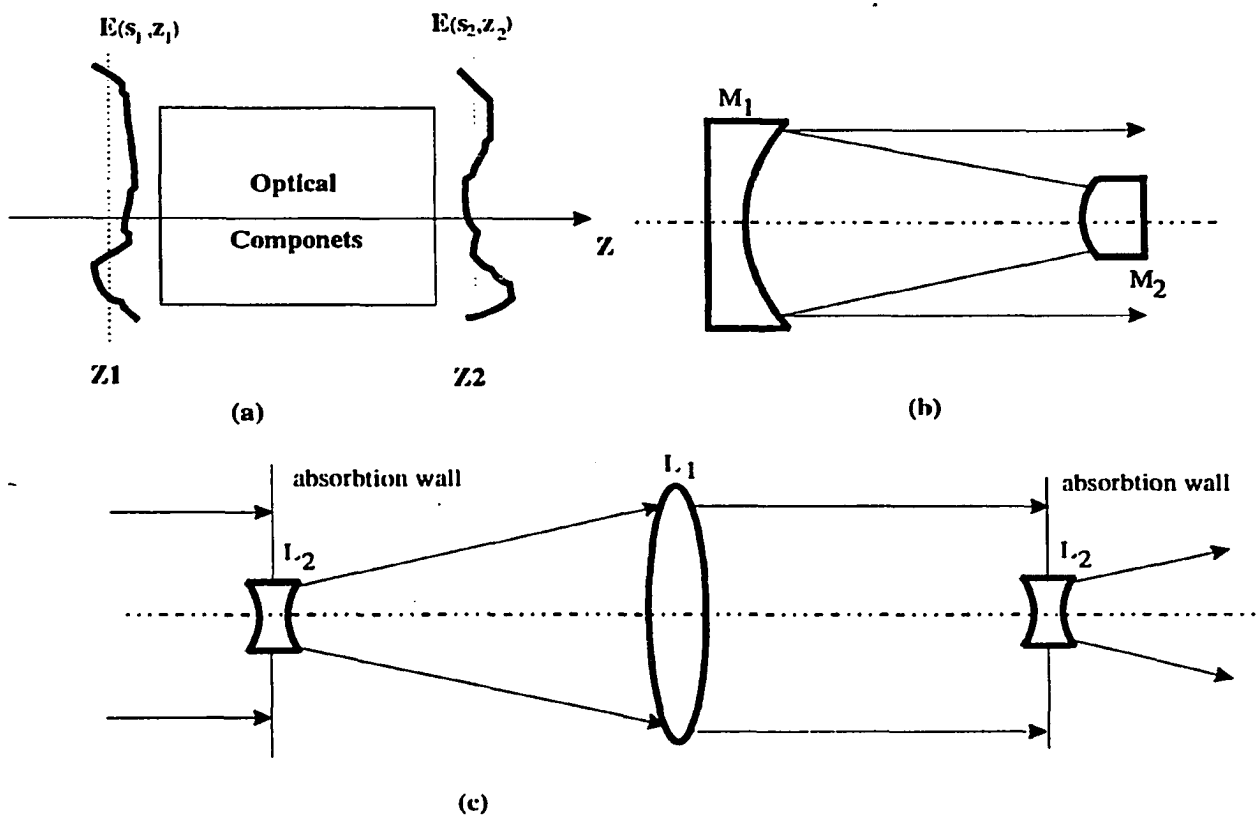

Figure 2. Diffraction optics treatment of an unstable resonator. (a) electrical field propagating from z_1 plane to z_2 through a set of optical components which can be represented by an integral kernel $K(z_1, z_2, s_1, s_2)$, (b) an unstable resonator, (c) a lens guide representing the unfolded cavity of (b).

For an realistic laser cavity, due to the necessary output coupling, the operator $\int \times K(z_1, z_2, \bar{s}_1, \bar{s}_2) d\bar{s}$ is Non-Hermitian in general. As an result, the eigenstates $\{u_n\}$ will be a non-orthogonal set:

$$\int u_n(\bar{s}, z) u_m^*(\bar{s}, z) d\bar{s} \neq \delta_{nm} \tag{13}$$

Instead, they are biorthogonal to their adjoint eigen-modes $\{\phi_m\}$:

$$\int u_n(\bar{s}, z) \phi_m(\bar{s}, z) d\bar{s} = \delta_{nm} \tag{14}$$

The adjoint set $\{\phi_m\}$ is the optical eigen-modes of the lens guide propagating in the opposite direction of $\{u_n\}$ and they satisfy following eigen-equation:

$$\gamma_n \phi_n(z, \bar{s}) = \int \phi_n(z, \bar{s}') \times K^T(\bar{s}, \bar{s}') d\bar{s}' \tag{15}$$

where the $K^T(\bar{s}, \bar{s}')$, the transpose of $K(\bar{s}, \bar{s}')$, is the propagation kernel of the same lens guide but in the opposite direction of z.

With proper choice of the normalization conditions, we can prove that:

$$\phi_m(\bar{s}) = \frac{u_m(\bar{s}) e^{-i\alpha s^2}}{\int u_m^2(\bar{s}') e^{-i\alpha s'^2} d\bar{s}'} \tag{16}$$

where the integral plane $\bar{s}$ is located at the arbitrary position inside the resonator, and α is a factor depending on the symmetry of the integral plane $\bar{s}$ relative to the resonator's

geometrical configuration. At the symmetry plane, α=0 and the normalization of $\phi_m(\bar{s})$ at such plane can be obtained by using Eq. (15):

$$K_T^m = \int \phi_m(\bar{s})\phi^*{}_m(\bar{s})d\bar{s} = \frac{\int |u_m(\bar{s})|^2 d\bar{s}}{\left|\int u_m^2(\bar{s})d\bar{s}\right|^2} \tag{17}$$

Where the integration is carried out at the plane of symmetry. This factor is a very important in determining the spontaneous emission enhancement for transverse mode $u_m(\bar{s})$ as will be discussed in the next section.

II-3) Excess Spontaneous Emission Factor

To derive the relation of the modal orthogonality and the excess spontaneous emission factor, we consider a laser resonator which has the properties discussed in previous section, i.e. that the field inside the resonator is governed by equation (6) and the resonator has a set of biorthogonal transverse modes $\{u_n(\bar{s})\}$ and their adjoint $\{\phi_m(\bar{s})\}$, which has all the properties of (13)-(17).

The electric field $E(\bar{r},t)$ inside such resonator, which is built upon the spontaneous emission noise, is expanded in terms of these eigen-modes of the resonator. Our goal is to derive the equations which govern the temporal behavior of the expansion coefficients and determine the spontaneous emission factor of each mode from the corresponding rate equation. The electric field $E(\bar{r},t)$, in the presence of the spontaneous emission noise source $P(\bar{r},t)$, is expressed in terms of $\{u_n\}$ as:

$$E(\bar{r},t)=\sum_n A_n(z,t)\gamma_n e^{[\ln(1/\gamma_n)z/p]}u_n(\bar{s},z)$$
$$=\sum_n A_n(z,t)e^{[(\bar{\alpha}-\alpha_n-i\beta_n)(z-p)]}u_n(\bar{s},z) \qquad (18)$$
$$A_n(z+p,t)=A_n(z,t)$$

Where the eigenvalue γ_n of u_n is written in form of $\gamma_n=e^{(\bar{\alpha}-\alpha_n-i\beta_n)p}$. $\bar{\alpha}$ is the cavity gain coefficient averaged along the resonator axis, and α_n and β_n are the amplitude and phase of γ_n. Notice that the effects of transverse gain-guiding has been taken into account in determining the eigenmodes $\{u_n\}$, so the $\{u_n\}$ has all the information about transverse gain. The advantage of using the formulation (18) is that, with the periodic boundary condition imposed on $A_n(z, t)$, each term in the expansion individually satisfies all the boundary conditions of the laser resonator. The periodic condition of $A_n(z, t)$ is guaranteed by further writing it as:

$$A_n(z,t)=\sum_q c_{qn}(t)\exp\{i\omega_{qn}t-i2\pi qz/p\}$$
$$\omega_{qn}=2\pi qc/p+\beta_n c \qquad (19)$$

By using equations (7),(18) and (19) and the biorthogonality relation of the resonator modes, the temporal evolution of the expansion coefficient $c_{qn}(t)$ is obtained:

$$[\frac{d}{dt}-c(\bar{\alpha}-\alpha_n)]c_{qn}(t)=-ip_{qn}(t)$$
$$p_{qn}(t)=\frac{\omega c\eta_0}{2p}e^{-i\omega_{qn}t}\int_0^p dz e^{i2\pi qz/p}e^{-(\bar{\alpha}-\alpha_n-i\beta_n)(z-p)} \qquad (20)$$
$$\times\int P(\bar{r},t)\phi_n(\bar{s},z)d\bar{s}$$

Equation (20a) is an equation driven by the Langevin noise source $p_{qn}(t)$ which represents the spontaneous emission. Comparing to the atomic emission wave length and the time constant of laser system, $p_{qn}(t)$ can be considered as delta correlated in both time and space. From the classical radiation theory and the biorthogonality relations (13)-(17), it can be shown that the $P(\bar{r},t)$ and $p_{qn}(t)$ has following auto-correlation:

$$\begin{aligned}
&\langle P(\bar{r},t)P(\bar{r}',t')\rangle = \frac{16\hbar\bar{\alpha}}{\omega\eta_0}\frac{N_2}{N_2-N_1}\delta(t-t')\delta(\bar{r}-\bar{r}') \\
&\langle p_{qn}(t)p_{qn}(t')\rangle = N_0\delta(t-t') \\
&N_0 = \left[\frac{\omega c\eta_0}{2p}\right]^2 \frac{1-|\gamma_n|^2}{2\bar{\alpha}|\gamma_n|^2}\frac{16\hbar\bar{\alpha}}{\omega\eta_0}\frac{N_2}{N_2-N_1}K_T^n
\end{aligned} \tag{21}$$

where the K_n^T is defined as in (17). With the knowledge of (21), the Langevin Equation (19) can be, after taking the assemble average, written as :

$$\frac{dn_{qn}}{dt} = \kappa N_2(n_{qn}+K_{qn}) - \kappa N_1 n_{qn} - \gamma_c n_{qn} . \tag{22}$$

The physical meaning of each term in (22) is explained as follow:

The photon number of the mode: $n_{qn} = \frac{\varepsilon}{2\hbar\omega}\frac{1-|\gamma_n|^2}{2\alpha_n}\langle c_{qn}c^*_{qn}\rangle$

Coupling term between atoms and cavity mode : κ

Spontaneous emission enhancement factor: $K_{qn} = K_T^n \times K_L^n$ (23)

$$\text{Longitudinal enhancement factor } K_L^n = \frac{1}{|\gamma_n|^2}\left[\frac{1-|\gamma_n|^2}{2\alpha_n p}\right]^2 \tag{24}$$

Transverse enhancement factor:

$$K_T^n = \int \phi_n(\bar{s})\phi^*{}_n(\bar{s})d\bar{s} = \frac{\int |u_n(\bar{s})|^2 d\bar{s}}{\left|\int u_n^2(\bar{s})d\bar{s}\right|^2} \quad \text{(at the plane of symmetry)} \tag{25}$$

Comparing to the conventional laser photon rate equations, the spontaneous emission power into the lasing mode, which is represented by the term of $\kappa N_2 K_{qn}$ in Eq.(22), is now multiplied by a factor K_{qn} . This enhancement of the spontaneous-emission factor is solely due to non-power-Orthogonality of resonator modes, i.e. the non-Hermitian properties of the resonator's operator. The resonator loss and out-put coupling along the longitudinal direction of the resonator (i.e. the end mirror loss) results in the enhancement factor K_L^n . On the other hand, the biorthogonality of transverse modes take the responsibility of K_T^n of Eq. (25).

In summary, for an optical resonator with a set of non-power-orthogonal eigen-modes, the spontaneous emission power entering a lasing mode will be enhanced by a factor comparing to that of a set of orthogonal modes. The cavity loss, the cavity geometrical structure and the cavity wave guiding mechanism can lead to the non-power-orthogonality of the resonator and thereby create the enhancement of the spontaneous emission factor.

III. Experimental Apparatus

To verify the theory of SEEF discussed in the previous section and to explore quantitatively how the laser mode properties can be affected by the cavity geometry and waveguide mechanism, we choose an unstable resonator semiconductor laser with lateral gain-guide for our experimental study. The experimental study of such system focus on measurement of SEF and the properties of the lasing mode (under different injection conditions) such as: far-field beam characteristics, lasing spectrum, transient response, and thermal wave guiding.

The physical structure of the unstable resonator semiconductor laser is shown in Figure 3. The material of the laser is the vertically integrated three-element phase locked laser array. Each element is a graded-index separate confinement single-quantum-well laser. With all three elements are identical, the out-of-phase mode normally dominates. To ensure the in-phase operation, the thickness of the quantum wells in the array are chosen to be 75Å, 100Å and 75Å respectively so that the in-phase mode has the highest gain. The vertical array considerably reduces the far-field divergence from 45° typical of the single-element laser to 25°. The threshold current density of the vertical-integrated array in the Fabry-Perot cavity is 2.5 times that of the individual element so that the current density per element is less than that of the single element. The power density of catastrophic optical damage is two times of that of the individual element.

The unstable cavity has a planar-convex configuration. The convex-end-mirror is fabricated by chemically-assisted ion-beam etching and the other end-mirror is a planar facet formed by natural cleavage. The radius of curvature of the convex mirror is 2.2 mm. This unstable geometry results in a magnification of 6.9. The gain medium is 100-μm wide

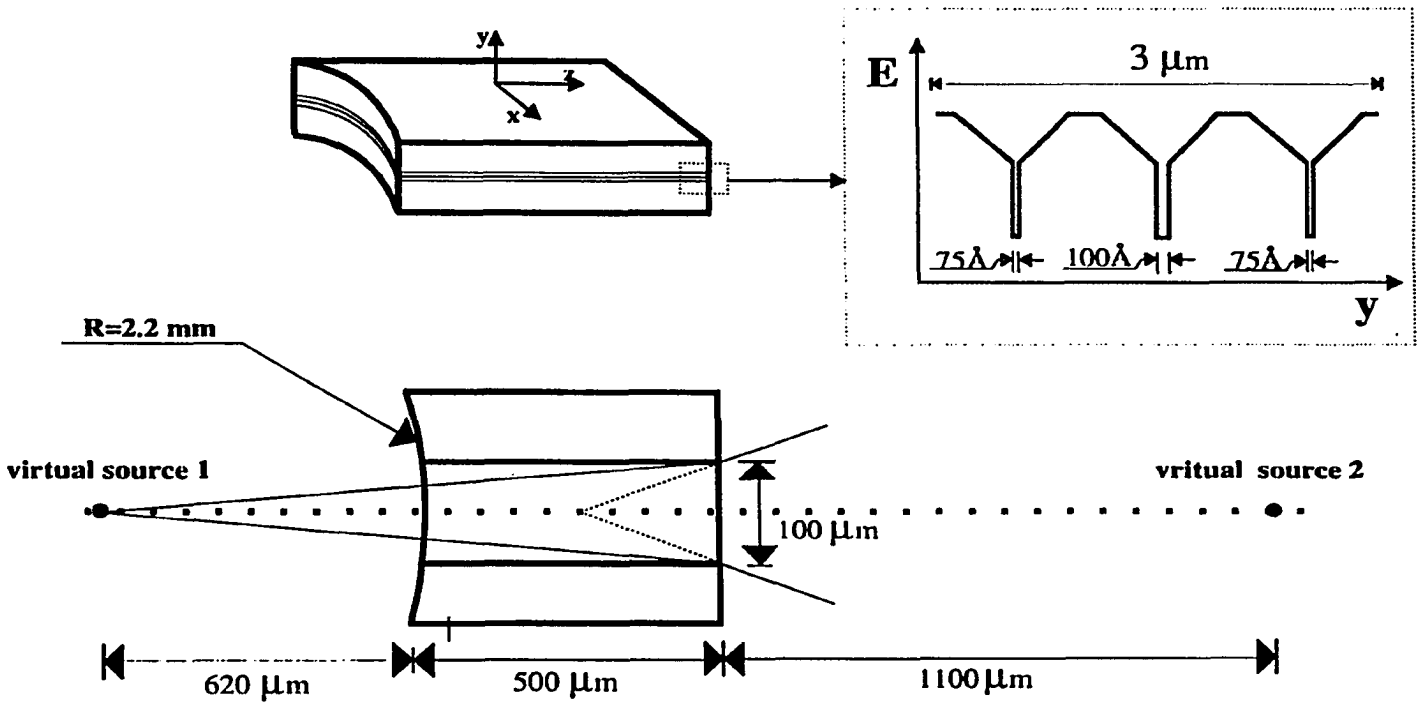

Figure 3. Physical structure of the unstable resonator semiconductor laser used in the experimental measurement.

and 500-μm long. The threshold current of the unstable resonator laser is 300 mA under CW injection operation and 750 mA under pulsed operation.

By applying geometrical resonator optics, the resonator's virtual sources obtained are located at:

$$d_1 = L(1+\sqrt{1+R/L})$$
$$d_2 = L\sqrt{1+R/L} \qquad (26)$$

where d_1 and d_2 is measured from the two mirror facets respectively as shown in Figure 3, L is the cavity length and R is curvature radius of the convex mirror. The laser output end is on the planar-mirror side. From the geometrical calculations, the virtual source viewed from the side of the planar mirror should be located at 0.31 mm behind the facet. This is in close agreement with the observed astigmatism of 0.3 mm when the laser is operated in the pulsed condition. This also indicates that the laser resonator is indeed operating in the unstable region as designed and that, at least near the center, the laser mode is determined by the geometrical structure of the unstable resonator.

The far-field intensity patterns of the lasing mode of the resonator under pulsed and CW operations are shown in Figure 4(a) and 4(b). The lateral far-field patterns in the pulsed operation (Figure 4(a)), measured at a 1.1 cm distance in front of the plane facet without any imaging optics, typically exhibit two lobes with many peaks in between whose intensity envelop has a depression at the center. In contrast to the pulsed operation, the laser far field is single-lobed with a much narrower divergence of less than 10° under the CW operation (Figure. 4(b)). In the pulsed operation, the multiple peaks in the far-field pattern are believed to be caused by the aberration when the wave front in the wings deviates considerably from the cylindrical (Gausian) shape as a result of the propagation in

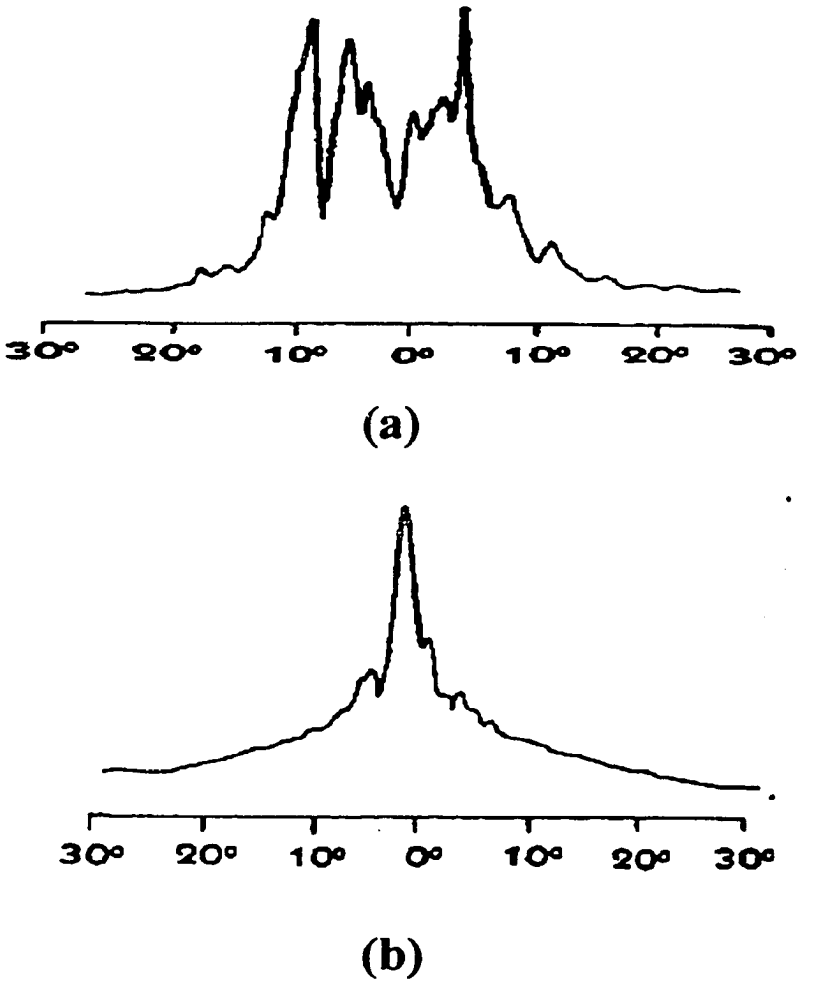

Figure 4. Far-field intensity of the unstable resonator semiconductor laser under (a) pulsed current injection and (b) CW current injection.

the lossy region outside the strip. Our numerical simulation to be presented later confirms this interpretation.

It should be pointed out here that, using the conventions commonly used in the literature of semiconductor lasers, the "near-field" in this paper refers to the lateral field distribution at the plane mirror facet and at the virtual source while the "far-field" refers to the laser output field from the plane mirror facet at some distance far away without any imaging optics. This definition of the near- and far- field is different from the one discussed by other previous authors[5-6].

The intensity profile at the virtual source and at the planar face under pulsed operation are shown in Figure 5(a) and 5(b). The near-field is obtained by projecting the magnified image of the facet on a detector array. Because the wave front in the direction perpendicular to the junction plane is planar while the wave front in the junction plane is curved, the output of the unstable resonator laser is astigmatic.

The thermal effect has significant influence on the lasing spectrum. Under the pulsed operation with 400-ns-long electric pulses, the unstable-resonator laser operates in a large number of longitudinal modes with adjacent modes clearly separated by 0.35 nm. Figure 6. shows the lasing spectra of the unstable resonator laser and a Fabry-Perot laser. A detailed examination of the spectrum reveals no signature of fine structures for unstable resonator laser. In contrast, the longitudinal-mode spectrum of a Fabry-Perot laser with comparable dimension exhibits fine structures and asymmetry owing to the multi-transverse modes operation. The clean spectrum indicates that the unstable cavity has effectively discriminated against the higher-order spatial modes and the laser operates in a single-transverse-mode. The unstable resonator laser has a much narrower longitudinal-

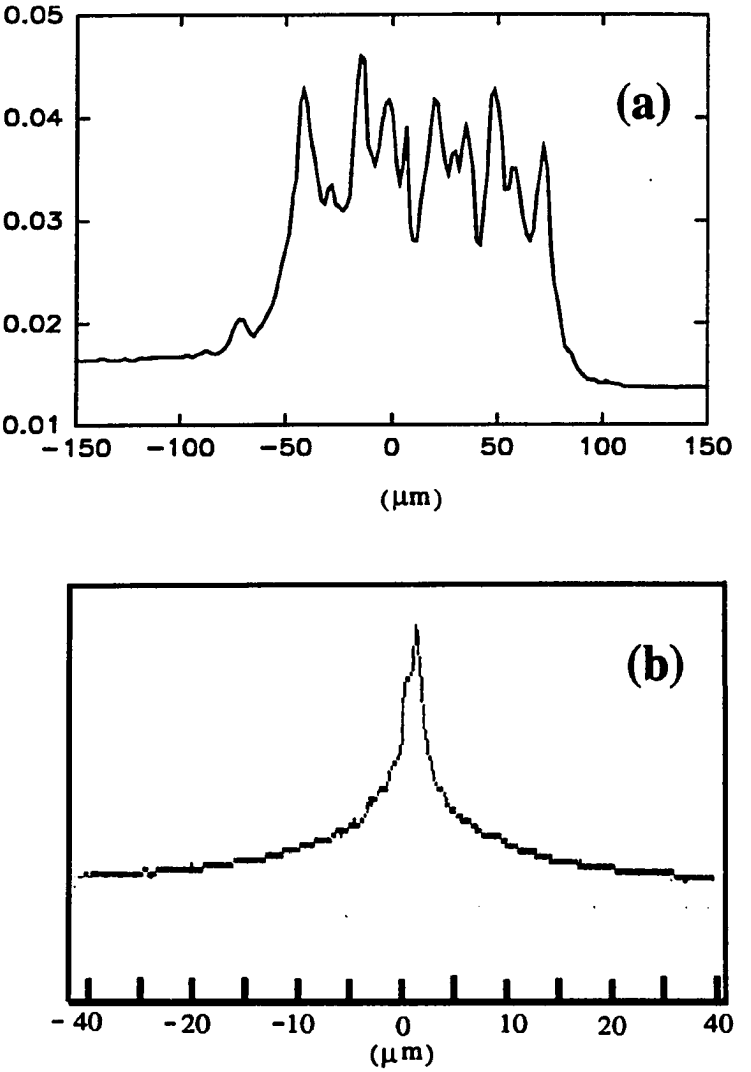

Figure 5. (a) Measured near-field intensity profile at the plane mirror facet of unstable resonator. (b) The field intensity profile at the virtual source.

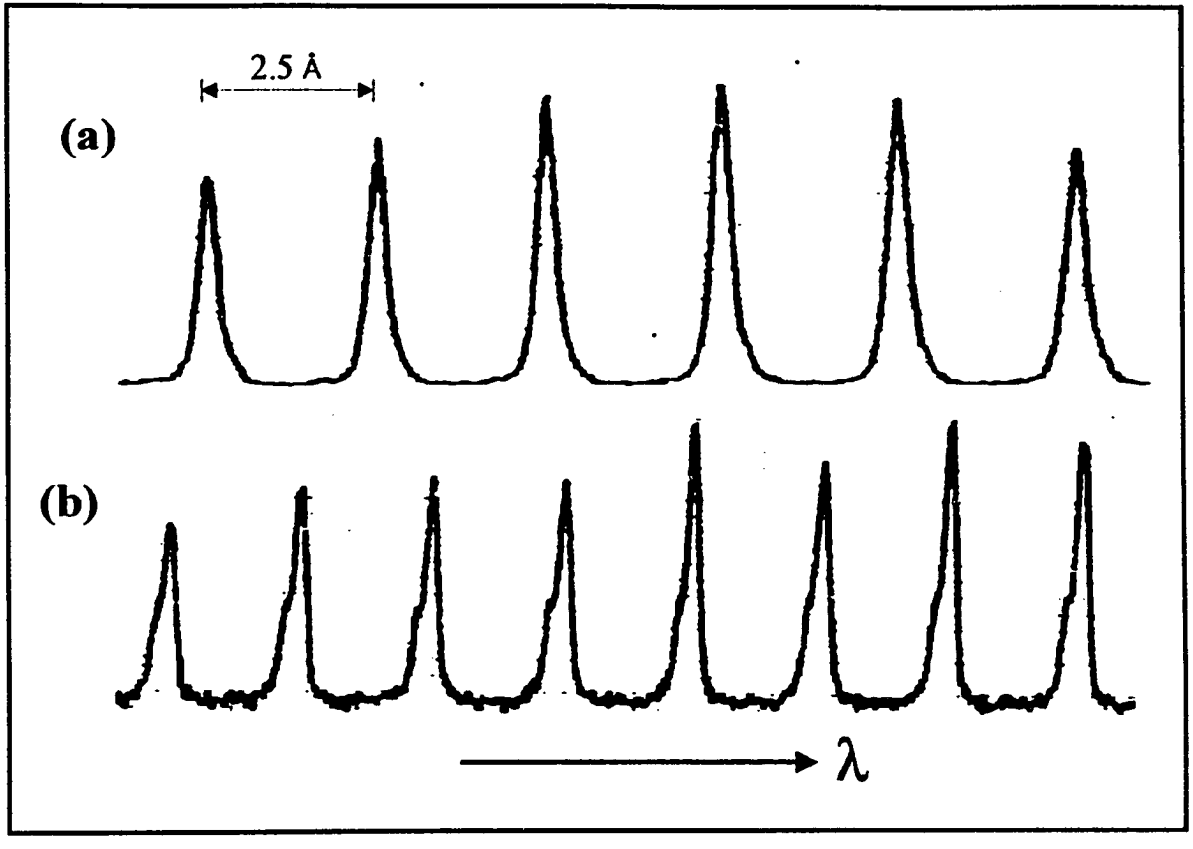

Figure 6. (a) The lasing spectrum of the unstable resonator semiconductor laser with 100-μm stripe width, (b) The lasing spectrum of a Fabry-Perot resonator semiconductor with the same stripe width.

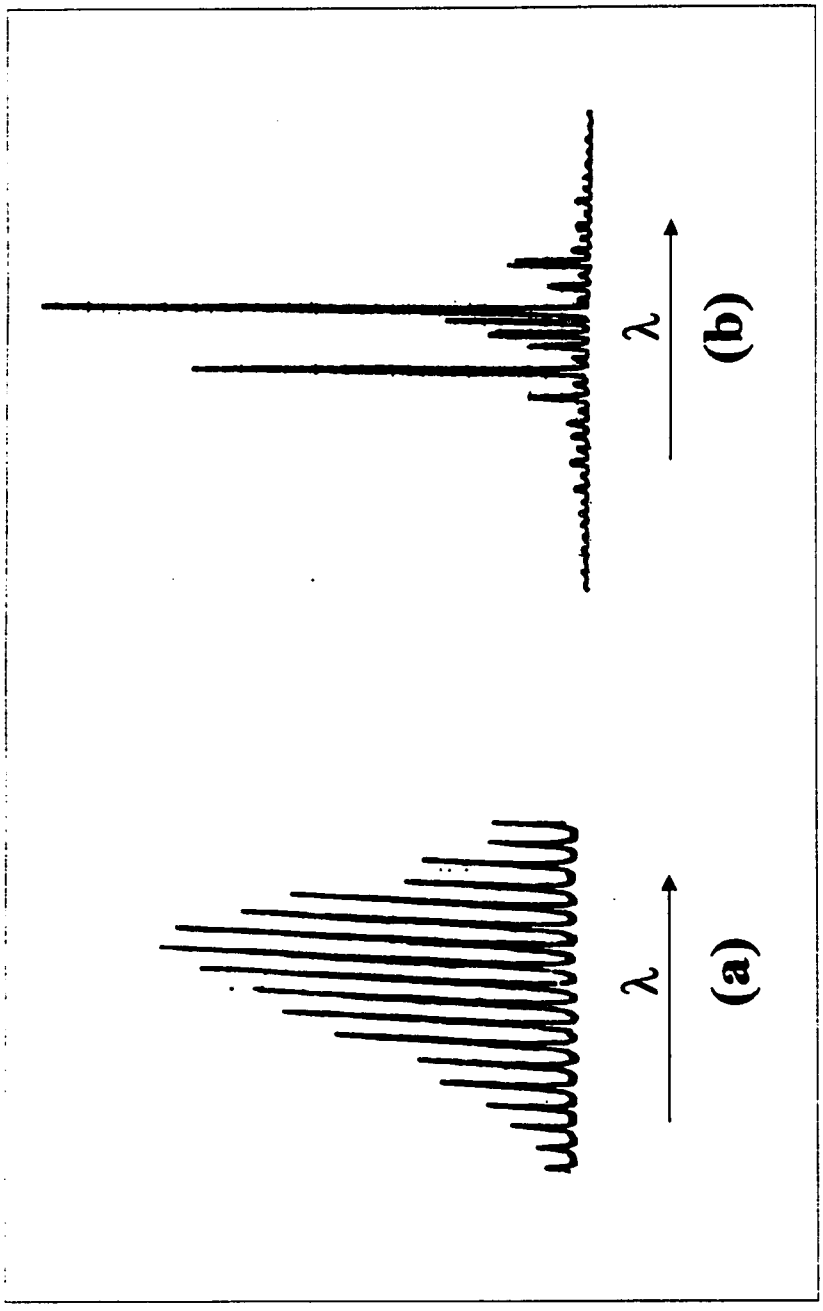

Figure 7. The lasing spectrum of unstable resonator semiconductor laser under (a) pulsed current injection and (b) CW current injection.

spectrum-width when it is in CW operation than in pulsed operation as it is shown in Figure 7.

The dramatic change of the laser beam character between the CW and pulsed operation is attributed to the formation of thermal-wave-guiding when the laser is pumped by CW current. The high injection current along active layer's lateral direction formed a thermal graded-gradient resulting in a equivalent gradient-index lens. The effect of the thermal lens results in partially canceling the beam divergence caused by the convex mirror curvature of the resonator and making the resonator more "stable". A time-resolved far-field measurement shows that, as a long current pulse is applied, the beam divergence slowly decreases with time as the temperature gradient increases.

The dynamic response of the unstable-resonator semiconductor laser is tested by driving the laser with fast-rising step like electric pulses and the laser output signal is recorded by a fast-detector and a fast sampling oscilloscope. A digital camera is used for recording. The transient responses for the unstable resonator laser and for a regular Fabry-Perot cavity laser of similar dimension are shown in Figure 8. (a) and (b) respectively. The rise-time of the current pulses is less than one nanosecond. For the Fabry-Perot laser, the relaxation oscillation has been clearly detected as shown in Figure 8 (a). On the other hand, the unstable resonator configuration has completely compressed the relaxation oscillation. In general, the decay time of the relaxation oscillation of a laser is determined by up-level population decay rate and the spontaneous emission factor of the system. The first factor is a property of laser material. The second factor is influenced by both the laser wave-guide mechanism and the resonator's geometrical configuration as discussed before. As it will be discussed in the next section, the suppression of relaxation oscillation of unstable resonator laser is indeed caused by unstable geometrical structure of the resonator.

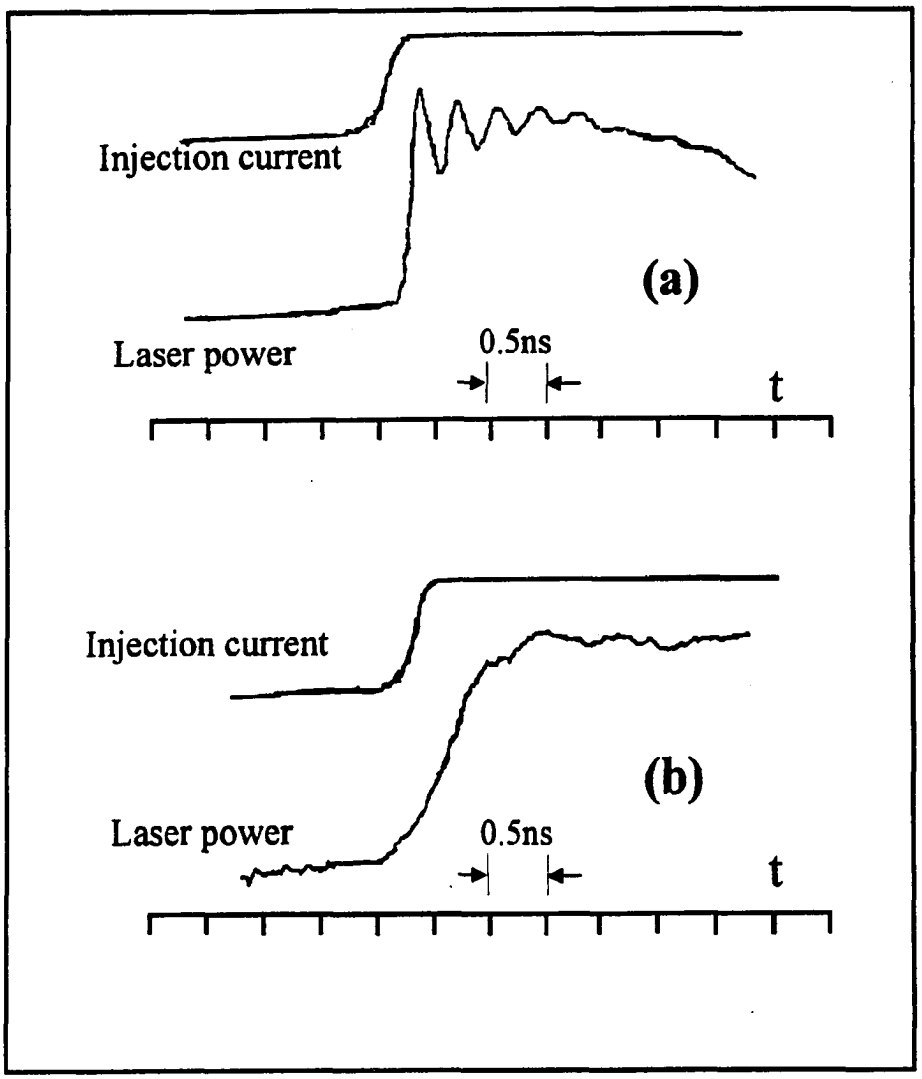

Figure 8. Transient response to a step-function-like injection current by a Fabry-Perot laser (a), and the unstable resonator resonator laser (b).

IV. Experimental Evaluation of Spontaneous Emission Factor

IV-1) *Determination of spontaneous emission factor by the power-current relation of the lasing mode.*

Our first approach for measuring the spontaneous emission factor, β, is to obtain experimentally the relation of the power per-mode as a function of the pumping current and to estimate the factor β by comparing the data with a set of calculated curves based on the multi-mode rate equations for various spontaneous emission factors. The method was first used by Suematsu , *et al.* [17] for the same purpose. Figure 9. shows the schematic of the experimental setup. The laser output was collected by a lens with numerical aperture 0.6 and sent to grating spectrometer with a 0.2 Å resolution. The slit opening of the spectrometer is adjusted so that the power of only one of the longitudinal modes near the peak of the gain profile is collected. A photo-multiplier is mounted on the output slit of the spectrometer and the photo current is sent to the recording unit. The measurement was conducted in both CW and pulsed condition. Under pulsed operation, the signals from the photo-multiplier are averaged by using a box-car integrator. The pumping electric pulse is 400-ns-long at a repetition rate of 200 Hz. The experimental results are shown in Figure 10. The current is normalized to the threshold current.

To estimate the spontaneous emission factor of the unstable resonator laser, we calculated the modal power versus current relation which are shown as the solid curves in Figure 10. The calculation is based on the following multi-mode rate equations with the assumption that the gain spectrum can be approximated by a quadratic profile [19]:

$$\frac{dP_m}{dt} = (G_m - \alpha)P_m + \beta\gamma_e N$$
$$\frac{dN}{dt} = \frac{I}{q} - \gamma_e N - \sum_m G_m P_m \qquad (27)$$

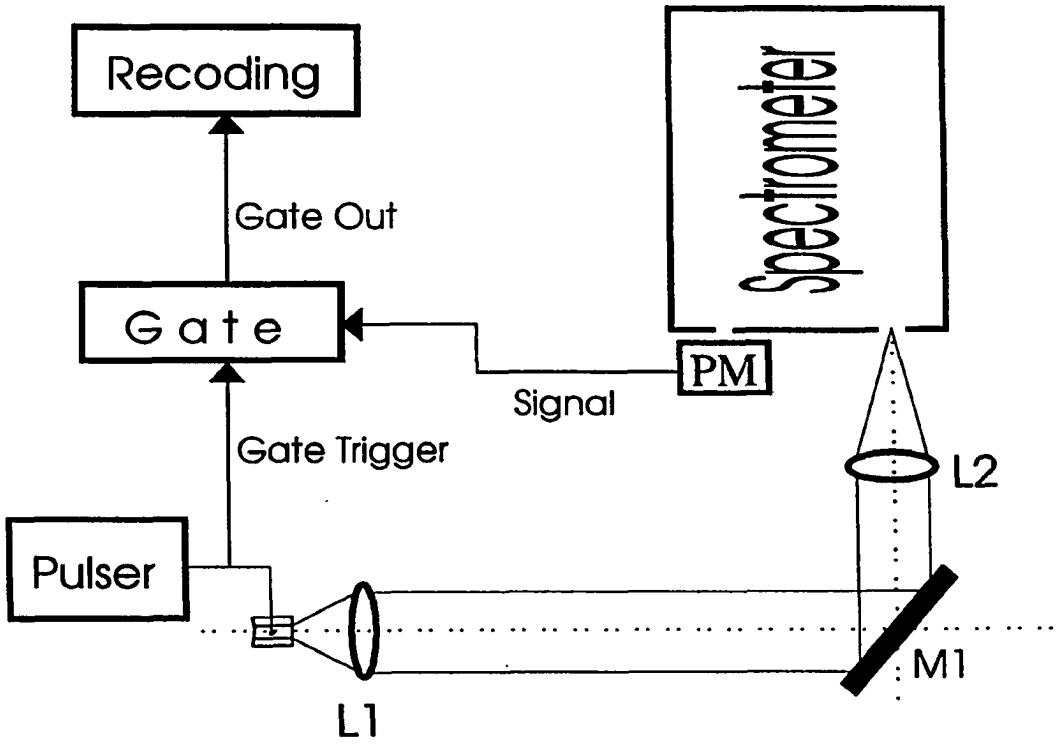

Figure 9. Experiment setup for the measurement of the spontaneous emission factor of the unstable resonator semiconductor laser.

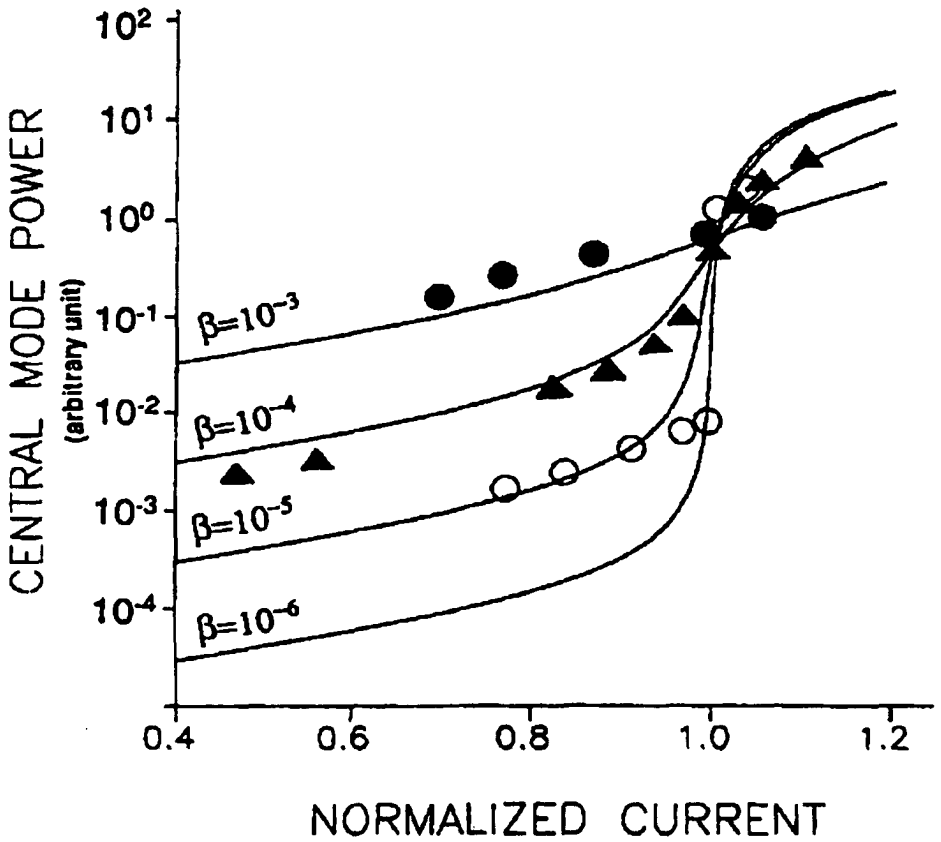

Figure 10. Output power of the central mode near the peak of the gain spectrum as a function of normalized injection current for the unstable-resonator semiconductor laser operated in the pulsed (filled circles) and CW (open circles) conditions, and for a 5-μm-wide ridge-guide Fabry-Perot laser (triangle). The solid curves are the results calculated based on the rate equations for various spontaneous emission factor.

Where:

P_m = photon number of m^{th} mode,

$G_m = G_n(N-N_0)(1-(m/M)^2)$ = gain of m^{ht} mode, $m=0,\pm1,\pm2\cdots\pm M$,

M = the total number of lasing modes within the gain spectrum,

$G_n = \partial G/\partial N$= the increment of gain with respect to total carrier number N,

α = cavity loss,

N = carrier number,

I = pumping current,

q = unit charge,

$\gamma_e = (A+BN+CN^2)$ = carrier decay rate,

$\beta = \beta_0 K_L K_T$ = spontaneous emission factor,

$\beta_0 = \lambda^4/4\pi^2 V_{eff}\Delta\lambda_{sp} n^3$,

The steady state relation of P_m and I is solved from the Eq. (27) and the P_0-I curves for various values of β is plotted in the Figure 10 as the solid lines. In the calculation, the total number of modes within the full width of the lasing spectrum is assumed to be 100, based on the experimental data.

We have also measured the relation of power-per-mode vs. current for a 5-μm-wide index-guided Fabry-Perot laser under the pulsed operation. The data are plotted in the Figure 10 as the filled triangles. A narrow-strip rather than a wide-strip Fabry-Perot laser is chosen in order to avoid the multimode operation, a situation that will complicate the measurement. Since the spontaneous emission factor is inversely proportional to the modal volume, the power vs. current relation for a 100-μm-wide Fabry-Perot cavity laser is expected to be between the solid lines corresponding to $\beta=10^{-5}$ and 10^{-6}.

Thus, from the Figure 10, we can draw the following conclusions. (1) By comparing the experimental data with the calculated curves, the spontaneous emission factor is determined to be 2×10^{-3} for pulsed operation and 1×10^{-5} for CW operation. Comparing to a Fabry-Perot cavity laser with same dimension, the spontaneous emission factor for the unstable resonator is 500 times larger in pulsed operation. (2) Under the CW operation, the spontaneous emission factor of the unstable resonator laser is drastically reduced. This is attributed to the development of thermal wave-guiding in the lateral direction, which changes the divergence of the beam in the unstable resonator. For the Fabry-Perot cavity laser, no considerable difference is found in the relation between the pulsed and CW operation.

IV-2) *Determination of spontaneous emission factor by the width of the lasing spectrum*

The spontaneous emission factor has also been measured by studying the width of the lasing spectrum envelope as a function of injection current. A grating spectrometer scans the laser emission power in both CW and pulsed operation. In pulsed pumping, the signal from the PM is sent to the box-car and gated relative to the leading edge of pumping pulse. A chart-recorder plots the spectra for various pumping levels. The measurement has been done for a unstable resonator laser and a regular Fabry-Perot laser with comparable dimensions. The measured widths of the lasing spectra as a function of pumping current are shown in Figure 11. The gradual decrease of spectra width with increasing pumping levels is observed for unstable resonator while the spectra width of the Fabry-Perot resonator exhibits a nearly abrupt reduction as the threshold is approached. Due to the larger spontaneous emission factor of the mode, as the pumping level close to the threshold, the mode growing speed change drastically and the acceleration depends the mode's location within the gain spectrum. The relative difference of growing speed between the central mode (mode at the peak gain) and side modes are greatly

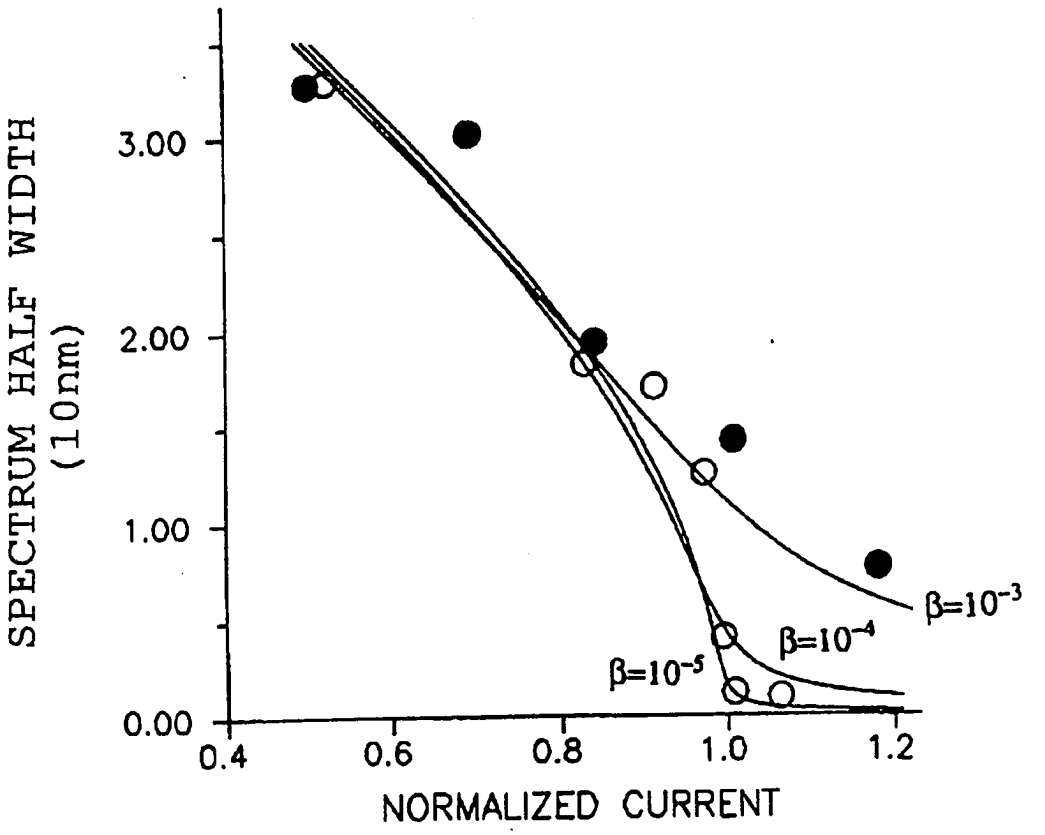

Figure 11. Half-width of the laser spectral envelope as a function of injection current for the unstable-resonator laser in the pulsed (filled circles) and CW (open circles) operation. The solid lines are the calculated results for various spontaneous emission factors.

influenced by the spontaneous emission factor, which tends to reduce the relative growing speed difference between the modes.

The calculation of the relation of the spectral envelope vs. the injection current can be carried out by obtaining the steady-state solution of equation (27). Assuming that the gain spectrum can be expressed as:

$$G(\omega) = G_0\left[1-\left(\frac{\omega-\omega_0}{\Delta\omega_g}\right)^2\right] \tag{28}$$

where the ω_0 is the central frequency of gain spectrum.$\Delta\omega_g$ is the gain spectrum half width and $G_0 = G_N(N-N_0)$. The steady-state photon number of each mode is

$$P_m = \frac{\beta\gamma_e N}{\alpha - G(\omega)} \tag{29}$$

Substitute (28) and (29) into the steady-state equations of Eq.(27), we can obtain the spectral half width as:

$$\Delta\omega_s = 2\Delta\omega_g\left(\frac{\delta}{1-\delta}\right)^{1/2}$$
$$\delta = \frac{\beta\gamma_e N}{\alpha P_0} \tag{30}$$

where the $\Delta\omega_g = 2\pi M(c/2L)$ (31)

and 2M +1 is the number of longitudinal cavity modes for which the gain is positive.

The calculated $\Delta\omega_s$ verse pumping current relations for the unstable resonator under both pulsed and CW injections are shown in Figure 11. By comparing with the calculated solid line in Figure 11, the spontaneous emission factors for the unstable resonator laser are 10^{-3} and 10^{-5} for the pulsed and the CW operations. The results are in close agreement with the ones obtained through relation of mode-power vs. current. The measured results of β are summarized in the following Table 1. The result shows the two major factors that will change the spontaneous emission factor of an unstable resonator semiconductor lasers: Fabry-Perot cavity configuration and thermal waveguide.

Table 1. Summary of experimentally measured spontaneous emission factors in various conditions.

	Pulsed Operation	CW Operation
Unstable Resonator (100μm width)	$\beta=2\times10^{-3}$	$\beta=1\times10^{-5}$
F-P Resonator (5μm width)	$\beta=8\times10^{-5}$	$\beta=8\times10^{-5}$
F-P Resonator (100μm width)	$\beta=4\times10^{-6}$	$\beta=4\times10^{-6}$

IV-3) *Transient response of unstable resonator laser*

As mentioned before, one of the important dynamical features of the unstable-resonator semiconductor laser is that the relaxation oscillation is strongly damped. This is tested by driving the laser with a fast rising electric pulse and by detecting the output of laser light by a fast detector. The detector signal is then displayed using a high-speed sampling units. Figure 8 (a) and (b) shows the observed transient response of an unstable resonator laser and a Fabry-Perot resonator laser of comparable dimension. With the understanding that

unstable-resonator laser possesses a much laser spontaneous emission factor, we can now give an explanation of this dynamic behavior.

For a given value of the device current I, the steady-state solutions of the rate equations of (27) are readily obtained. Using the small-signal analysis, the rate equations (27) can be linearized by neglecting the quadratic and higher powers of δP and δN. We then obtain the following small signal equations[19]:

$$N=N_S+\delta N(t),\ P=P_S+\delta P(t)$$

$$\begin{aligned}\delta\dot{P} &= -\Gamma_p\delta P+(G_N P_s+\partial R_{sp}/\partial N)\delta N\\ \delta\dot{N} &= -\Gamma_N\delta N-(G+G_p P_s)\delta P\end{aligned} \tag{33}$$

where

$$\begin{aligned}\Gamma_P &= \beta N_s\gamma_c/P_s-G_P P_s\\ \Gamma_N &= \gamma_c+N_s(\partial\gamma_c/\partial N)+G_N P_s\end{aligned} \tag{34}$$

The relaxation damping term Γ_P is proportional to the spontaneous emission factor β. Thus, the strong damping effect of the relaxation oscillation in an unstable resonator is another direct evidence of high value of spontaneous-emission rate in the lasing mode.

In summery, our experimental study of unstable resonator semiconductor laser has uncovered the following features of the system:

1) The laser possess larger spontaneous emission factor due to its unstable geometric configuration. The enhancement factor of the spontaneous emission is two orders higher than that of the regular Fabry-Perot lasers with same gain volume.
2) The laser operates in multi-longitudinal mode due to enhancement of spontaneous emission factor.

3) The laser operates in the fundamental transverse mode due to the effective suppression of higher order modes in unstable cavity.
4) The Relaxation oscillation is strongly damped.
5) The development of the thermal wave-guiding when the laser operates with CW injection greatly changes the mode properties of the resonator and drastically reduces the enhancement factor of spontaneous emission.

V. Numerical Modeling

To quantitatively describe how the geometric configuration and gain guiding mechanism affect the modal properties and spontaneous emission factor, we have carried out a numerical modeling of a laser system. Both the unstable resonator geometric and the lateral gain profile have been taken into account. The laser modes calculated with different system parameters are then used to calculate the spontaneous emission factor based on the equation (1)-(3). The calculated results are compared with the experimental data so that the theory given in section II is further confirmed and the general relation between enhancement of spontaneous emission factor and system's parameters are discussed.

The complexity of unstable resonator geometry makes it impossible to obtain an analytical solution of the optical modes of the resonator. This is especially true for our case in which the optical mode of the resonator is determined by both the lateral gain profile and geometrical configuration of the end-mirrors, i.e. the optical mode of the resonator is formed through both active and passive guiding mechanism.. For this reason, the eigenmodes of the unstable resonator are solved numerically with the aid of computer modeling of the system. The earlier studies on the modal calculation of cold (or passive) unstable-resonator are mostly based on Fox-Li method [20-21] for either one or two

dimensions resonators. The basic principle of the Fox-Li method of modal calculation is that any arbitrary initial electric filed lunched into given resonator, after interacting long enough with the resonator's optical components, will settle down to one of the eigenmodes of the laser resonator that has the minimum of the round-trip loss and will reproduce itself in both phase and amplitude after each round trip. For an active gain-guided unstable semiconductor resonator, Lang, *et al.* [3] has treated the lateral guide and end-mirror effect separately for the mode calculation. In this approach of the active resonators, a complete knowledge of the analytic eigen-mode solution of the lateral gain guide must be obtained before solving the eigen-mode of the resonator as whole. For many situations, the complexity of the lateral gain distribution and dynamical behavior makes it impossible to get the analytic solution. Therefore this treatment of active cavity is limited to those resonator in which lateral gain profile can be approximated by either Gausian or Step-like function and without considering the dynamics of interaction between the gain and modal field.

In the following, we present our modal calculation of the active unstable resonator which takes into account the effect of both lateral gain guiding and curved mirrors at the ends. The numerical modeling is a beam- propagation method [18-19] based on the Fox-Li [20] algorithm. The method is useful for any arbitrary lateral gain profile and unstable geometrical configuration. It is assumed that the propagation of the resonator modes can be described by following paraxial-wave equation:

$$\frac{\partial u(x,z)}{\partial z} = \left(\frac{1}{2ik} \frac{\partial^2}{\partial x^2} + \frac{k(n(x)-1)}{2i} \right) u(x,z) \quad ; \quad E(x,z) = u(x,z) e^{ikz} \tag{35}$$

where k is the propagation constant, and u(x, z) is the field envelop which is slowly varying along z and x is in the direction perpendicular to the propagation.

The paraxial-wave assumption is justified by the following arguments. From the geometrical calculation of the unstable resonator mode, the fundamental mode of the cavity can be seen as two count-propagation spherical waves with their virtual sources located outside of the resonator, as shown in Figure 12 (a). For the parameters of the laser resonator used in the experiment, each of these two virtual sources sustain an angle less than 10^0. This condition of the resonator mode guarantees that the propagation of the mode field u(x, z) along the cavity axis satisfies the paraxial approximation condition:

$$\frac{1}{u(x,z)}\frac{\partial^2 u(x,z)}{\partial z^2} << 1 \qquad \text{or} \qquad \left|\frac{\partial^2 u}{\partial z^2}\right| << \left|\frac{\partial^2 u}{\partial x^2}\right| \tag{36}$$

To calculate the eigen mode of the resonator, we unfold the resonator into an equivalent infinitely long lens waveguide as represented in Figure 12 (b). The unfolded waveguide has a spatial period equal to the round-trip distance of the unstable resonator and has the phase-and-amplitude transformer representing the resonator's end-mirrors. The gain medium is extended along the z direction. In the lateral direction of the unfolded guide, a complex index profile is assumed to have the following spatial distribution:

$$\begin{aligned} n(x) &= \Delta n_R + i\, n_{IP}(x) \\ n_{IP}(x) &= \frac{n_{I0}}{e^{(|x|-w)/d}+1} \end{aligned} \tag{37}$$

where the Δn_R is constant of real part index and $n_{IP}(x)$ is the imaginary part of index induced by injection current, and d and w are the diffusion length and half maximum height width of the pumping gain. Figure 13 shows the spatial profile of the $n_{IP}(x)$ used in the modeling.

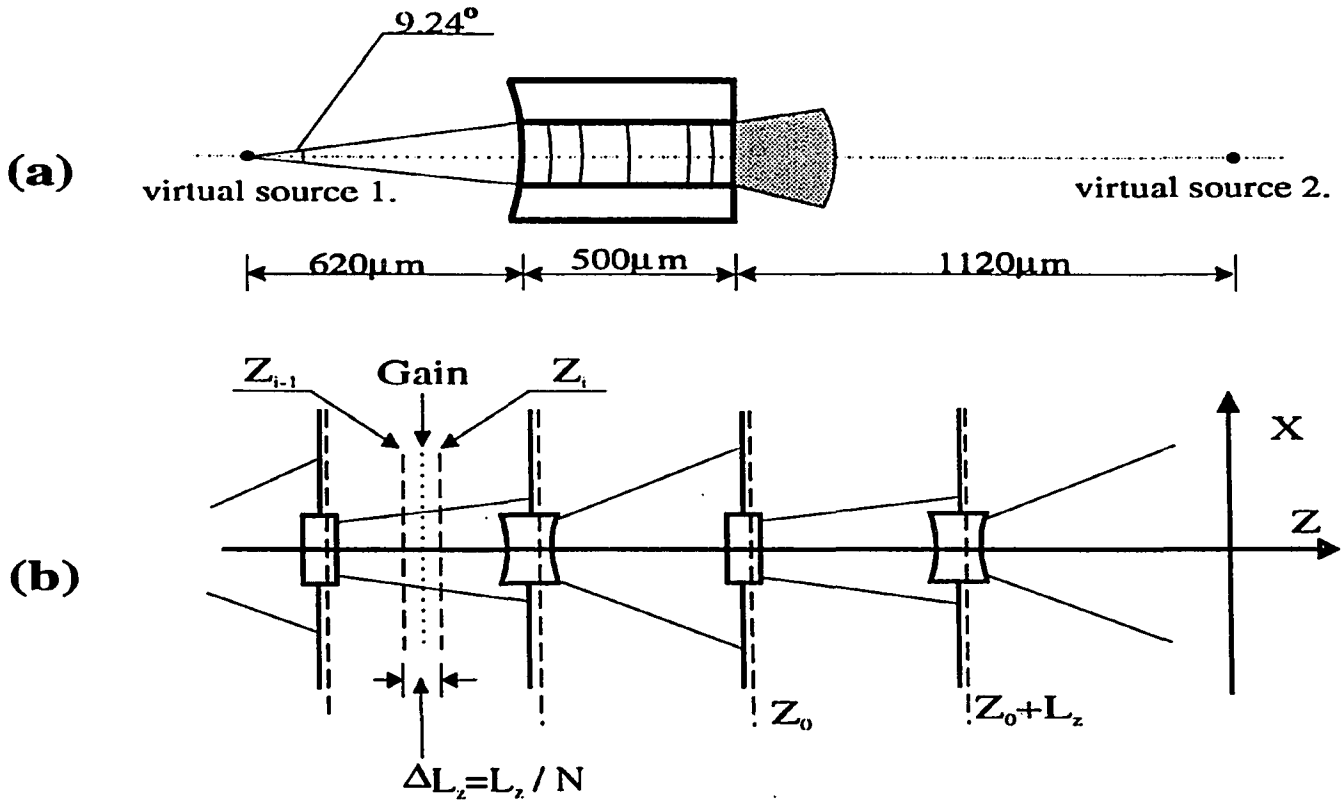

Figure 12. (a) The structure of the unstable-resonator semiconductor laser and (b) its unfold-lens-guide for numerical modeling. Within each spatial period of the lens guide, the space is divide into several sections with a gain sheet inserted in the middle of the section representing the lateral gain guide.

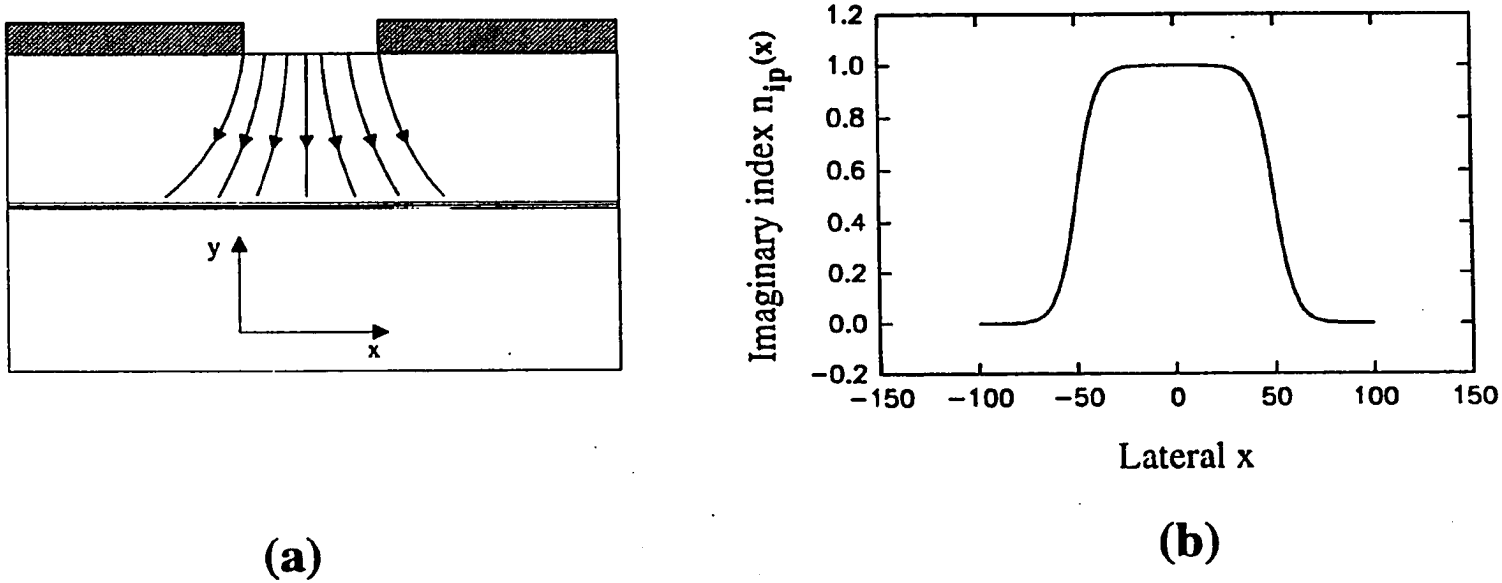

Figure 13. (a) Cross-sectional view of the unstable resonator semiconductor and (b) imaginary index profile induced by injection current in the lateral direction used for the modeling.

Each spatial period (which is equal to round-trip of the resonator) of the waveguide is divided into N segments, each having a length given by $\Delta L=L_Z/N$. The gain and diffraction effects of the wave propagating along the waveguide are treated separately. According to paraxial wave equation (35), with each increment step Δz, the field u(x, z) changes accordingly:

$$\frac{\partial u(x,z)}{\partial z} = (\hat{D}+\hat{G})u(x,z) \quad \text{or} \quad u(x,z+\Delta z) = u(x,z)[\exp(\hat{D}+\hat{G})\Delta z]$$
$$\hat{D} = (1/2ik)\frac{\partial^2}{\partial x^2} \quad ; \quad \hat{G} = \frac{kn_1(x)-1}{2i} \tag{38}$$

where $\hat{D}$ is the diffraction operator and $\hat{G}$ is the gain operator. To separating the gain and diffraction operators in the exponential part of (38), propagation operator $\hat{P}(\Delta L,\hat{D},\hat{G}) = \exp\{(\hat{D}+\hat{G})\times\Delta L\}$ of each segment will has, according to the argument given by [18], the minimum errors if the following sequence of operators is used:

$$u_i = \hat{P}(\Delta L,\hat{D},\hat{G})u_{i-1} = [\exp(\hat{D}\Delta L/2)][\exp(\hat{G}\Delta L)][\exp(\hat{D}\Delta L/2)]u_{i-1} \tag{39}$$

where the u_{i-1} is the field entering the i^{th} segment and u_i is the field at the end of segment. An initial field with arbitrary phase and amplitude spatial distribution is launched at z=0 plane. As it entering the each section, the field first propagating $\Delta L/2$ in free space and encounters a gain sheet represented operator $\exp(\hat{G}(x)\Delta L)$. The field then continues to propagate through the next $\Delta L/2$ free space until it reaches the next section.

The diffraction operator $\exp(\hat{D}\Delta L/2)$ propagating the field $u_i(x, z_i)$ in the free space with distance $\Delta L/2$. To save the computation time, the propagation of the field in the free space is done by Fast Furies Transform algorithm. The field $u_i(x, z_i)$ is decomposed into the

components of the paraxial-plane-waves with different k_x and the amplitude of each commonest is given by:

$$a(k_x, z_i) = \int u(x, z_i) e^{-ik_x x} dx \tag{40}$$

Each paraxial-plane-wave component with k_x will travels in free space from z_i to $z_i+\Delta L/2$ with different propagation wave vector k_z differently:

$$a(k_x,\ z_i + \Delta L/2) = a(k_x, z_i) \exp\{-i\Delta L/2(k_0 - k_x^2/2k_0)\} \tag{41}$$

The field is then reconstructed at $z_i + \Delta L/2$ according to:

$$u(x, z_i + \Delta L/2) = \int a(k_x, z_i + \Delta L/2) e^{ik_x x} dk_x \tag{42}$$

Process of (40) and (42) are done with Fast Furies Transform with 4096 grid points in lateral x space and k_x space. The gain operator $\exp(\hat{G}(x)\Delta L)$ acts on the field $u(x, z_i + \Delta L/2)$ to give rise to:

$$u'(x, z_i + \Delta L/2) = u(x, z_i + \Delta L/2) e^{ikn_I(x)\Delta L}$$
$$n_I(x) = \Delta n_R + i \frac{n_{IP}(x) - n_{Ib}}{1 + \left(|u_i|^2 / |u_{gs}|^2\right)} \tag{43}$$

Here $n_I(x)$ is the imaginary part of the index including the pumping induced n_{IP}, material background loss n_{Ib} and the gain saturation filed intensity $|u_{gs}(x)|^2$. The appendix A gives the derivation of this gain saturation field intensity $|u_{gs}(x)|^2$. The new field

$u'(x, z_i + \Delta L/2)$ propagates through the rest of segment until reaches the starting point of $(i+1)^{th}$ segment.

The effect of the curved end mirror is represented a phase and amplitude transform function:

$$\hat{M}(x) = re^{ik_0 n_R \delta(x)} \quad \text{with } \delta(x) = R\left(1 - \sqrt{1-(x/R)^2}\right) \tag{44}$$

Where R is the radius of mirror curvature $\delta(x)$ represents the phase shift upon the reflection on the mirror and r is field reflectivity of the end mirror. A complete round trip of the field propagation inside of the resonator is equivalent to the propagation of one spatial period along the unfolded wave guide:

$$U_{n+1}(x) = \hat{M}_1(x)\left(\prod_{i=1}^{N} \hat{P}_i(\Delta L, \hat{D}, \hat{G})\right)\hat{M}_2(x)\left(\prod_{i=1}^{N} \hat{P}_i(\Delta L, \hat{D}, \hat{G})\right)U_n(x) \tag{45}$$

Where $U_n(x)$ is the field after n^{th} round trip and N is total number of segments for each spatial period of $2L_z$. The criteria for the mode formation is test by the following condition about round-trip-power ratio η_i and cavity loss $1-|\gamma_n|^2$:

$$\lim_{n\to\infty} \eta_n = \lim_{n\to\infty}\left(\frac{\int |U_{n+1}(x)|^2 dx}{\int |U_n(x)|^2 dx}\right) = \text{constant, or, } \lim_{n\to\infty}|\gamma_n|^2 = \text{constant}$$

$$|\gamma_n|^2 = \eta_n \exp\{-4L_z\bar{g}\} \text{ ; and } \bar{g} = \frac{\int g(x)|U_n(x)|^2 dx}{\int |U_n(x)|^2 dx};\ g(x) = k_0 n_I(x) \tag{46}$$

where $U_{n+1}(x)$ and $U_n(x)$ is the field after and before the n^{th} round trip. The round trip loss $1-|\gamma_n|^2$ includes the power loss due to both diffraction and end mirrors' transmission. $g(x)=k_0 n_I(x)$ is the gain per-unit length. The pumping level is determined by the constant P_0 in Equation (37). This constant is first adjusted to a level so that the round-trip power ratio η_i is greater than unit, meaning that the gain overcomes the cavity's round-trip loss. The whole process of the mode formation takes place within a few round trips and both η_i and γ quickly approach to constant values. The details of computer program use Microsoft FORTRAN 5.0 are included in Appendix.

The modal field at the plane mirror facet is defined as near-field that reproduce itself after each round trip and this field distribution is used for far-field calculation. The Figure 14 presents the near- and far- field calculation for a 100-μm gain-strip unstable resonator with one of the convex mirror of 2.2 mm radius curvature. Comparing with the experimental observation of Figure 4 and Figure 5, the numerically calculated far-field pattern exhibits similar multi-peaks feature with a divergence of 15°. The near-field at the plane mirror facet is used to evaluate the transverse enhancement factor K_T of spontaneous emission factor according to Eq.(3). The longitudinal enhancement factor is calculated from Eq. (2) by using the γ obtained from Eq.(46). Using cavity length L_z=500 μm, R_2=2200μm, and the gain-strip width w=100μm, the numerically computed transverse and longitudinal enhancement factor of spontaneous emission are listed in Table 2.

Table 2. Calculated spontaneous emission factors

	K_T	K_L	K	β_0	β
Unstable Resonator (100 μm)	158	4.4	695.2	1.0×10^{-6}	6.9×10^{-4}
Fabry-Perot Resonator (100 μm)	1.11	1.2	1.32	1.0×10^{-6}	1.3×10^{-6}

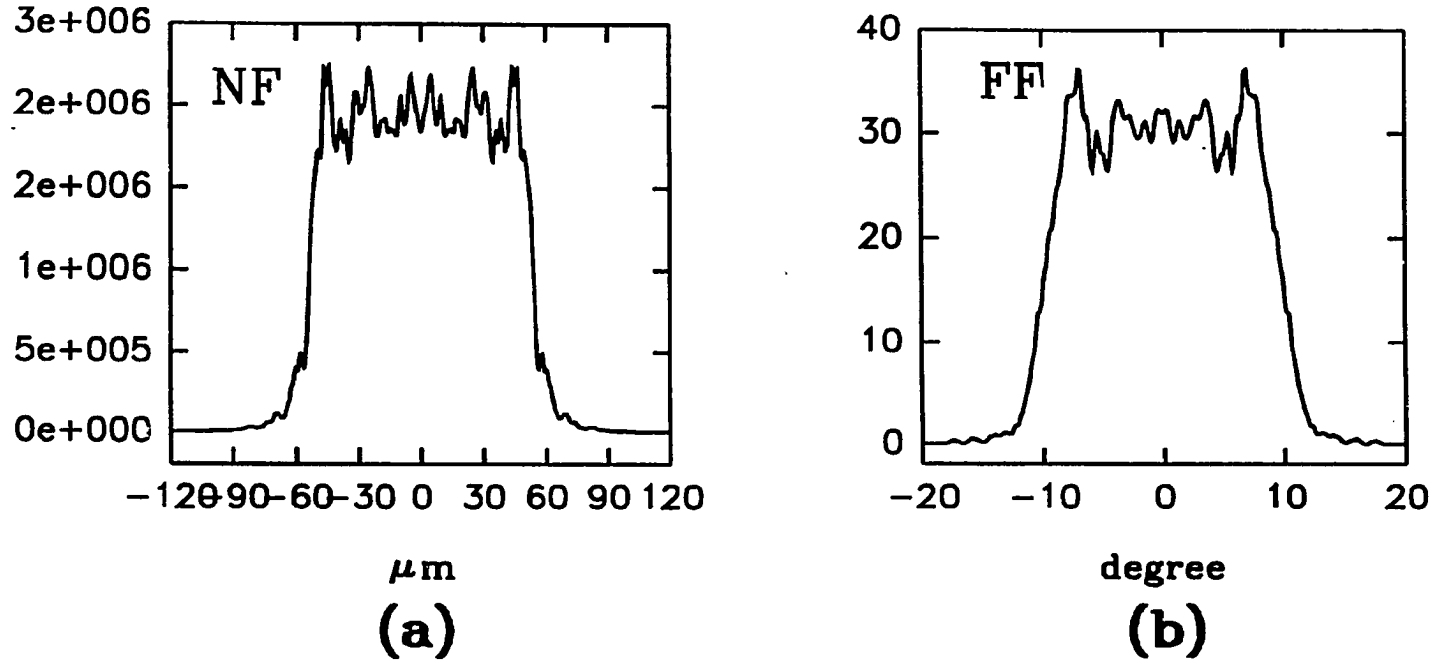

Figure 14. Numerically calculated (a) near-field intensity distribution at the plane of the mirror facet (b) the far-field intensity distribution.

From the previous experimental results in Table 1, the spontaneous emission factor for an unstable resonator mode without thermal lens effect (i.e. under pulsed operation) is on the order of 2×10^{-3} based on the comparison of experimental data and calculation of central mode power and injection current relation. On the other hand, by the same method, the spontaneous emission factor for a Fabry-Perot laser with same dimensions is obtained on the order of 4×10^{-6}. This corresponds to an enhancement factor of K=500 times. Our numerical modeling gives a good agreement on this matter.

In the previous paper [23], we have used far-field fitting method to evaluate the transverse enhancement factor of spontaneous emission. With far-field-fitting method, we assume the near field at the plane facet of unstable resonator can be approximated by a hyperbolic $\text{sech}^q(x)$ function, where $q=q_R+iq_I$ is a complex parameters. The q value is determined by the geometric of the cavity in a such way that the Taylor Series expansion of the field near x=0 gives rise to a cylindrical wave front that matches the radius curvature of the convex mirror of the resonator. The far-field is calculated with this assumed near field and compared with the experimental measurement. The K_T, evaluated based on this near field according to (3), is 175 which is very close to the one calculated here. Considering the fact that evaluation of q is totally based on the geometric parameters of the cavity without considering the lateral gain-guide, we can conclude that, for a broad stripe unstable resonator with lateral gain guide, the K_T is mainly determined by the geometric parameter R, the radius of curvature of the end-mirror.

To investigate how the resonator's geometrical parameters affect the enhancement factor, we plot the numerically calculated K, K_T, K_L verses cavity length L_Z, convex-mirror radius curvature R, and gain-strip width w in the Figures 15-18. For the calculations shown in the Figure 15, the radius of curvature of the convex mirror and the width of the

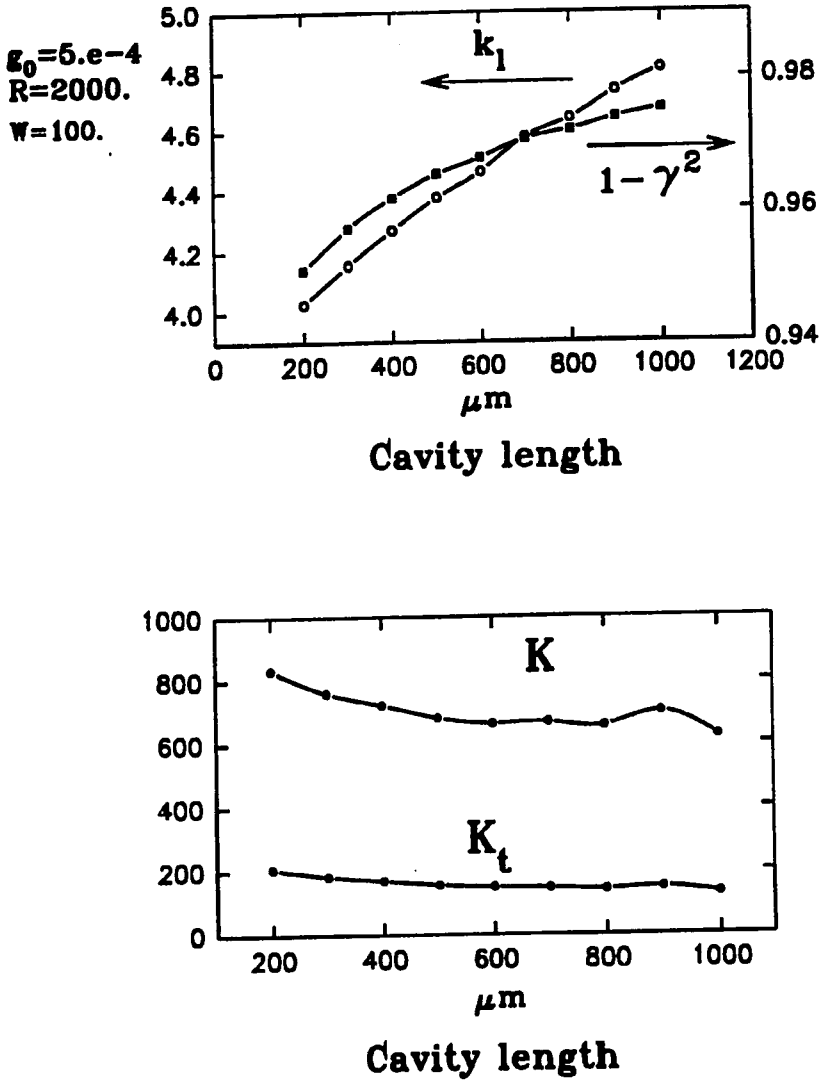

Figure 15. (a) Numerically calculated cavity round-trip loss 1- γ^2 and longitudinal enhancement factor K_l verse the cavity length. (b) Numerically calculated transverse enhancement factor K_t and total enhancement factor K verse the cavity length.

gain medium are fixed at 2000 μm and 100 μm respectively. The increase of cavity loss with the increase of cavity length is mainly due to the increasing magnification of unstable geometrical structure and results in a increase of longitudinal enhancement factor K_L. The total enhancement factor K which is the product of K_L and K_T remains fairly constant with the change of cavity length. This can be explained by the fact that for a broad strip unstable-resonator laser, the enhancement factor is mainly caused by the geometrical structure which, in this case, is mainly determined by the radius curvature R. The small peak of K at 700μm and 900μm cavity length is due to the diffraction effect which changes the mode magnification at certain critical geometrical parameters.

As mentioned earlier, although both the gain-guiding mechanism and unstable geometrical-configuration can result in a non-Hermitian lasing mode and therefore a transverse enhancement factor K_T, for a wide-strip-width laser, the K_T is mainly determine by the unstable geometrical structure. Thus the radius curvature R of the convex mirror is the key parameter in determine the K factor. The drastic change of K with the change of radius of curvature, shown in Figure 16, demonstrates this point. For small radius of curvature, the central portion of the electric field in the cavity experiences much less phase lag from the outer portion of the field upon the reflection from the convex mirror during the formation of the resonator mode. As a result, a more ' improper mode ' is formed in the sense that wave front of the mode is much more curved. The increase of the curvature of the modal field not only increases the diffraction loss but also increases the non-Hermitian components of the lasing mode and, as a result, both the K_L and K_T increase.

Finally, we analyze the effect of strip width on the spontaneous emission factor. It should be emphasized here again that, in the case of lateral gain-guided unstable-resonator laser, the non-Hermitian properties of the lasing mode is originated by two major causes, both

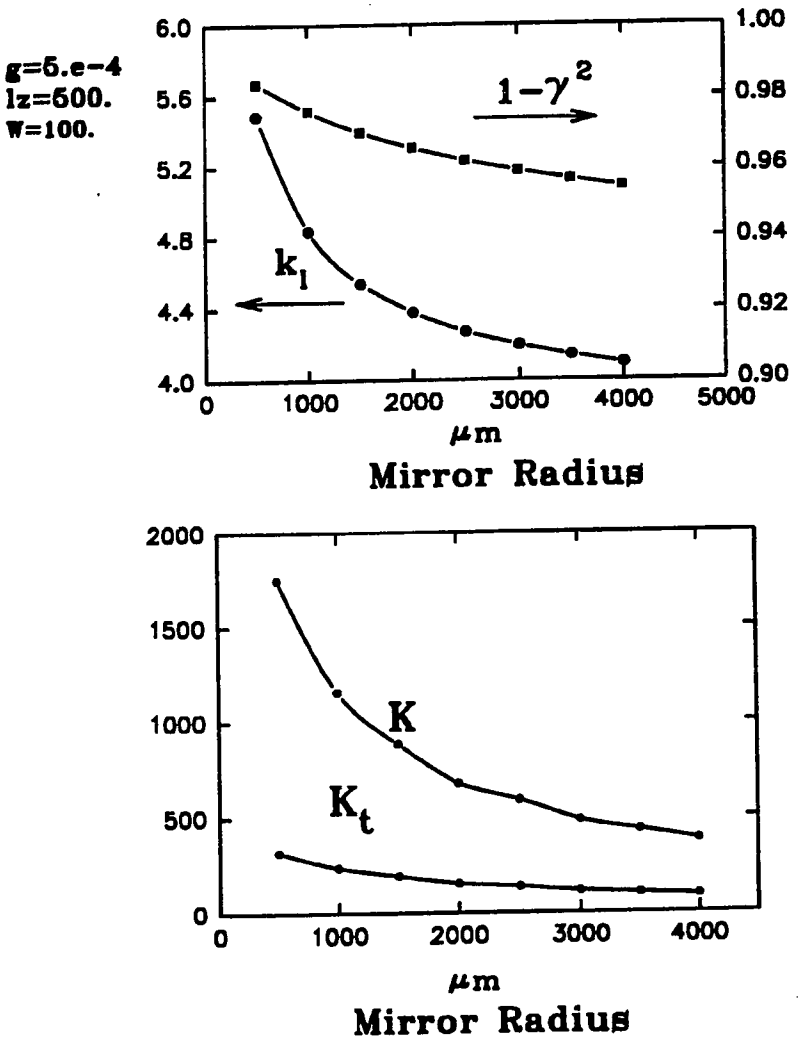

Figure 16. (a) Numerically calculated cavity round-trip loss $1-\gamma^2$ and longitudinal enhancement factor K_l verse the mirror radius of curvature. (b) Numerically calculated transverse enhancement factor K_t and total enhancement factor K verse the mirror radius of curvature.

gain-guiding mechanism and the unstable-geometrical structure of the resonator. These two causes play different roles depending on the resonator parameters. For broad strip width, the gain profile is largely uniform in the central portion and the modal property is mainly determined by the unstable geometry, as mentioned earlier. As the strip width becomes narrower to a few μm, for a mirror curvature of 2.2 mm, the modal field no longer experiences the unstable geometry upon reflecting from the convex mirror. The lateral gain-guiding starts to play a dominant role in determine the mode field and the non-Hermitian features of the mode. Consequently, for narrow strip width, the K factor is more sensitive to the lateral gain spatial profile and the gain distribution in lateral direction can no longer be modeled through equation (37) as in the case of wide-gain-strip laser. The carrier diffusion plays more important role in the formation of the cavity modes.

To deal with these matters, we investigate the behavior of the K factor for different range of gain-strip width with different spatial gain profile. From 20 μm ~ 110 μm strip width, we use equation (37) as the pumping induced lateral gain and the calculated results of K_L, K_T, and K are plotted in Figure 17. Again, the resonator loss factor $1-|\gamma|^2$ has a maximum peak at 35 μm width, which is due to the diffraction effect. The transverse enhancement factor decreases drastically with the decreasing strip width. This trend stops when the strip width is sufficiently narrow that modal field no longer experience much of the unstable geometry of the cavity due to the mirror curvature and the K value remains constant.

For the narrow strip width between 2 μm and 30 μm, we use following complex lateral index profile with a Gausian imaginary part (which represents the gain) in the numerical modeling:

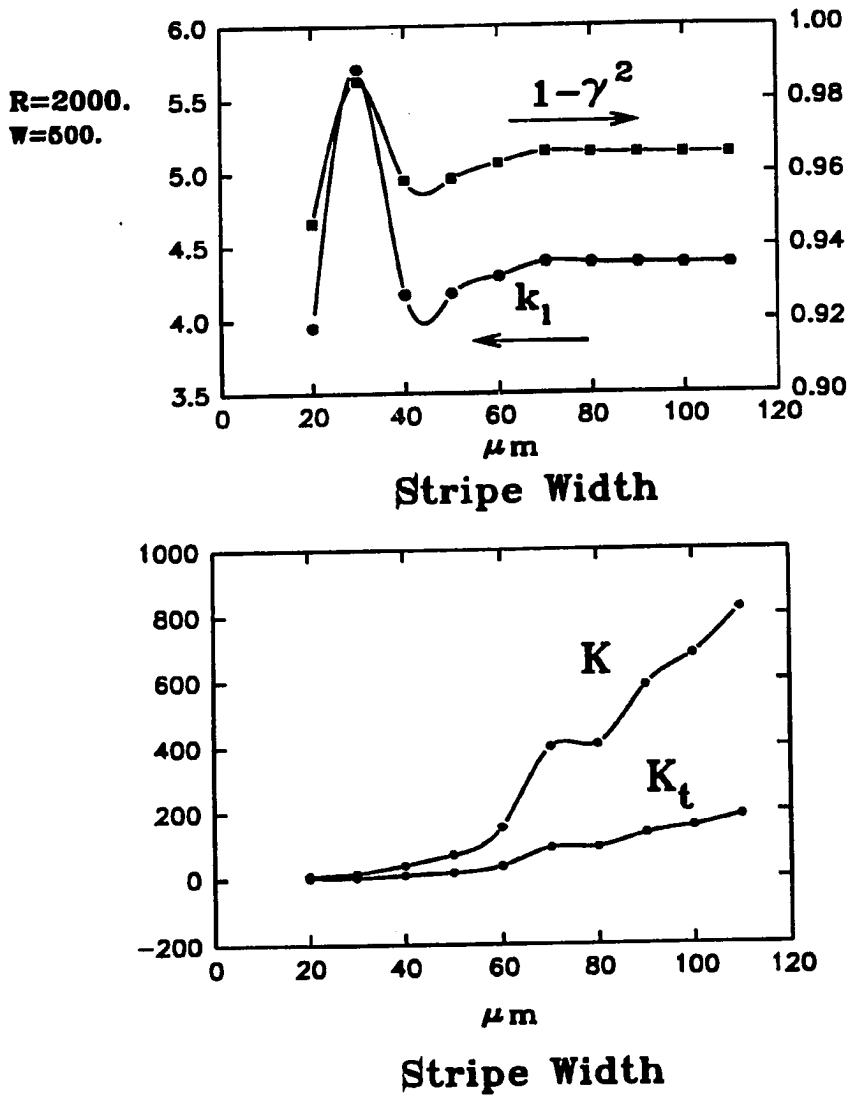

Figure 17. (a) Numerically calculated cavity round-trip loss 1- γ^2 and longitudinal enhancement factor K_l verse the stripe width w in the 20-100 μm range. (b) Numerically calculated transverse enhancement factor K_t and total enhancement factor K verse the stripe width w in the 20-100 μm range.

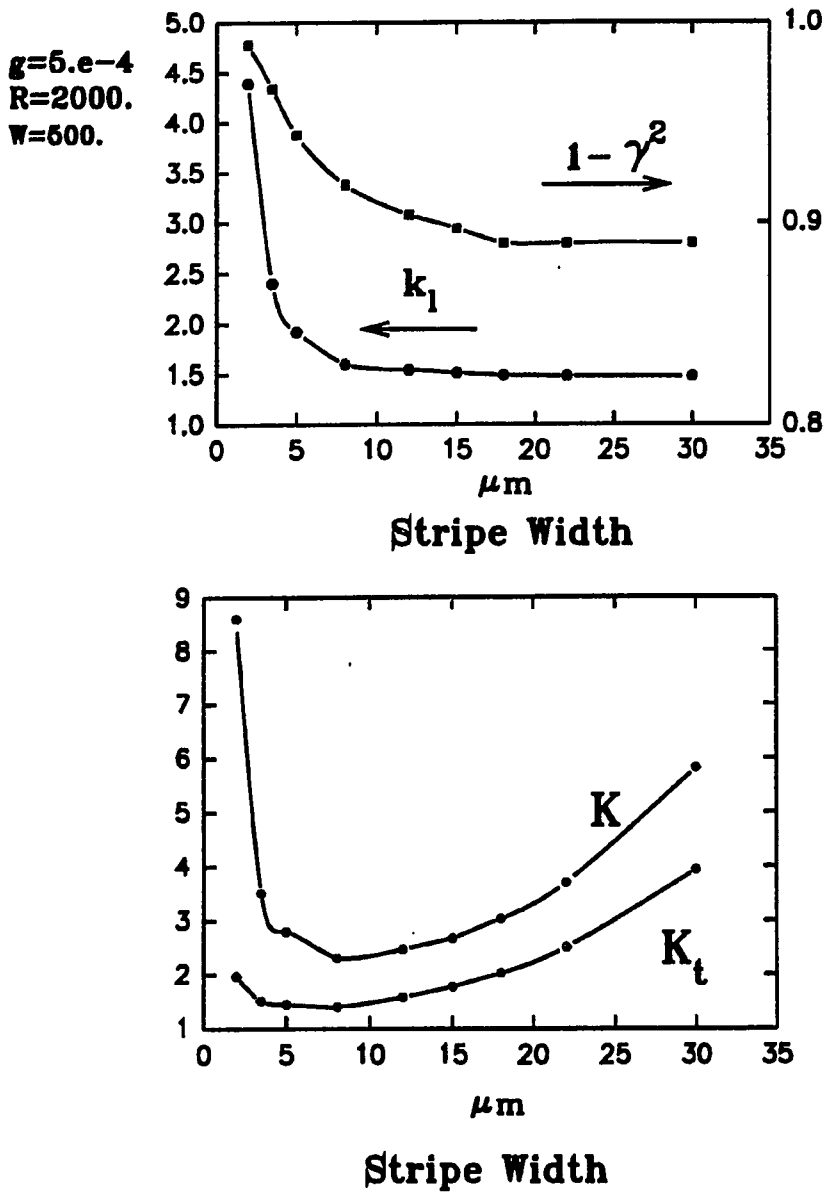

Figure 18. (a) Numerically calculated cavity round-trip loss 1- γ^2 and longitudinal enhancement factor K_l verse the stripe width w in the 2-30 μm range. (b) Numerically calculated transverse enhancement factor K_t and total enhancement factor K verse the stripe width w in the 2-30 μm range.

$$n_{IP}(x) = n_{I0}\exp(-ax^2)$$
$$a = \frac{\sqrt{4\ln(2)}}{w^2} \qquad (48)$$

Where n_{I0} is height of the gain and the width parameter w is regarded as the half width of the imaginary part of refractive index profile. The calculated values of K_T, K_L, and K for various strip width are plotted in Figure 18 with w=2μm , cavity length L_z=500μm, and mirror curvature R=2000 μm. . The transverse enhancement factor remains fairly constant in this region while the longitudinal enhancement factor changes drastically as the strip width decreases to less than 5μm. The fast increase of the cavity mode round-trip loss is the cause of the rapid growth of spontaneous emission enhancement factor for narrow strip width.

VI. Conclusions

In conclusion, we have studied the modal properties and determined the spontaneous emission factor of an unstable-resonator semiconductor laser with a planar-convex geometry. The open resonator configuration results in an enhancement by two orders of magnitude in the spontaneous emission factor. The development of thermal wave guiding under the CW operation results in a significant reduction in the spontaneous emission factor. We have observed a clear correlation between the spontaneous emission factor and the width of the lasing spectral envelope. With the large spontaneous emission factor, the unstable-resonator laser is dynamically stable against relaxation oscillations and other intensity instabilities. However, the development of thermal wave guiding can significantly affect the stability of the laser beam. The numerical modeling based on the beam-

propagation method shows that the enhancement factor of spontaneous emission is mainly due to the unstable geometry of the resonator while it is dominantly determined by the lateral gain mechanism when the strip width is less than 20 μm.

The enhancement factor of spontaneous emission K discussed here represents an increase in the spontaneous-emission rate into each cavity mode. This increased emission rate could lead to an increased noise additional to the "line width enhancement factor", α, discussed first by Henry [24] for semiconductor lasers. In a semiconductor laser, the spontaneous emission into the lasing modes will affect the phase fluctuations in two ways: both directly through the spontaneous emission events which shift the oscillation phase directly, and also indirectly through the intensity fluctuation that is translated into the phase fluctuation through amplitude-phase coupling. The Henry's line width enhancement factor is originated form intrinsic material properties of the semiconductor gain medium while the enhancement factor discussed here is the result of resonator geometrical configuration. Since the spontaneous emission is the cause of both effects, we expect the line width of the laser to be multiplied both by the excess spontaneous emission factor K discussed here and the $(1+\alpha^2)$ factor predicted by Henry. Hence the usual Schawlow-Townes laser line width should be enhanced by both factor.

Appendix

Modal Calculation of Unstable Resonator Semiconductor Laser:
Computer Simulation with FORTRAN Language.

Program Structure

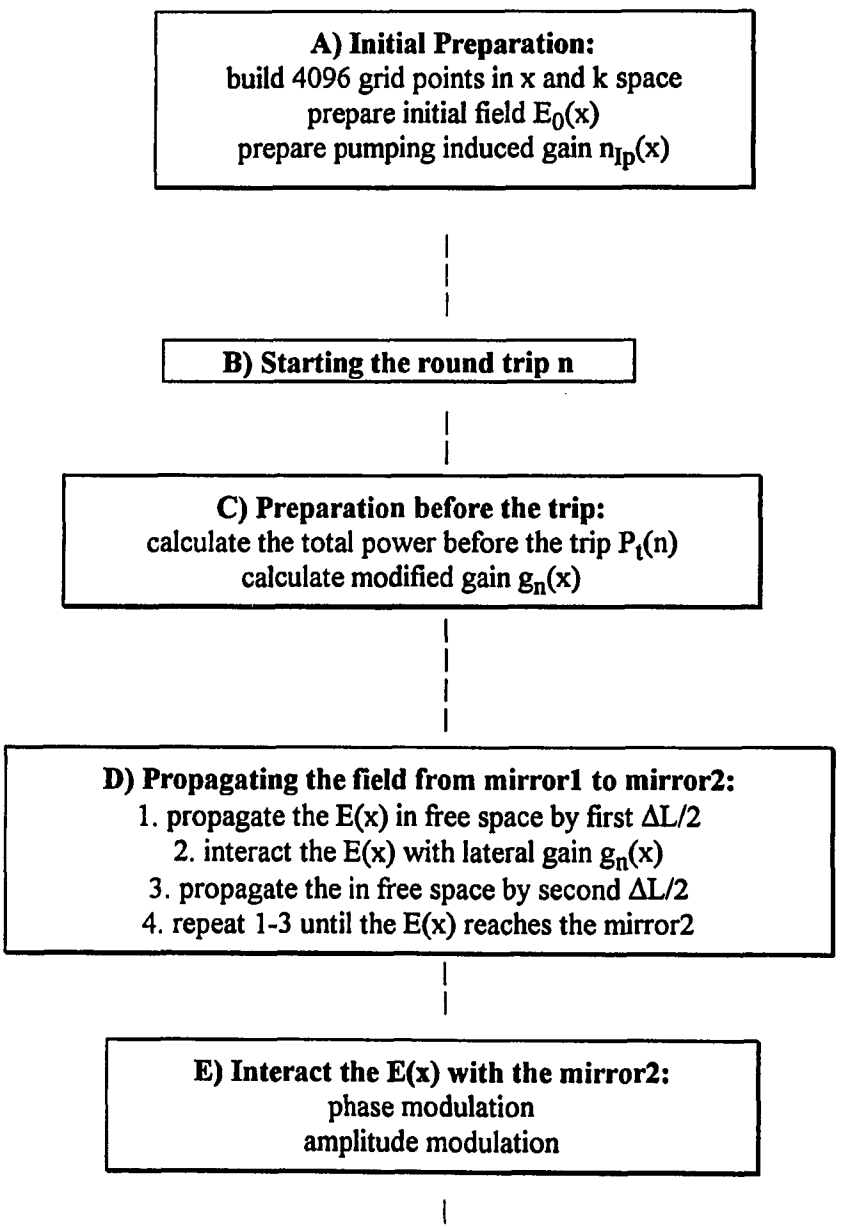

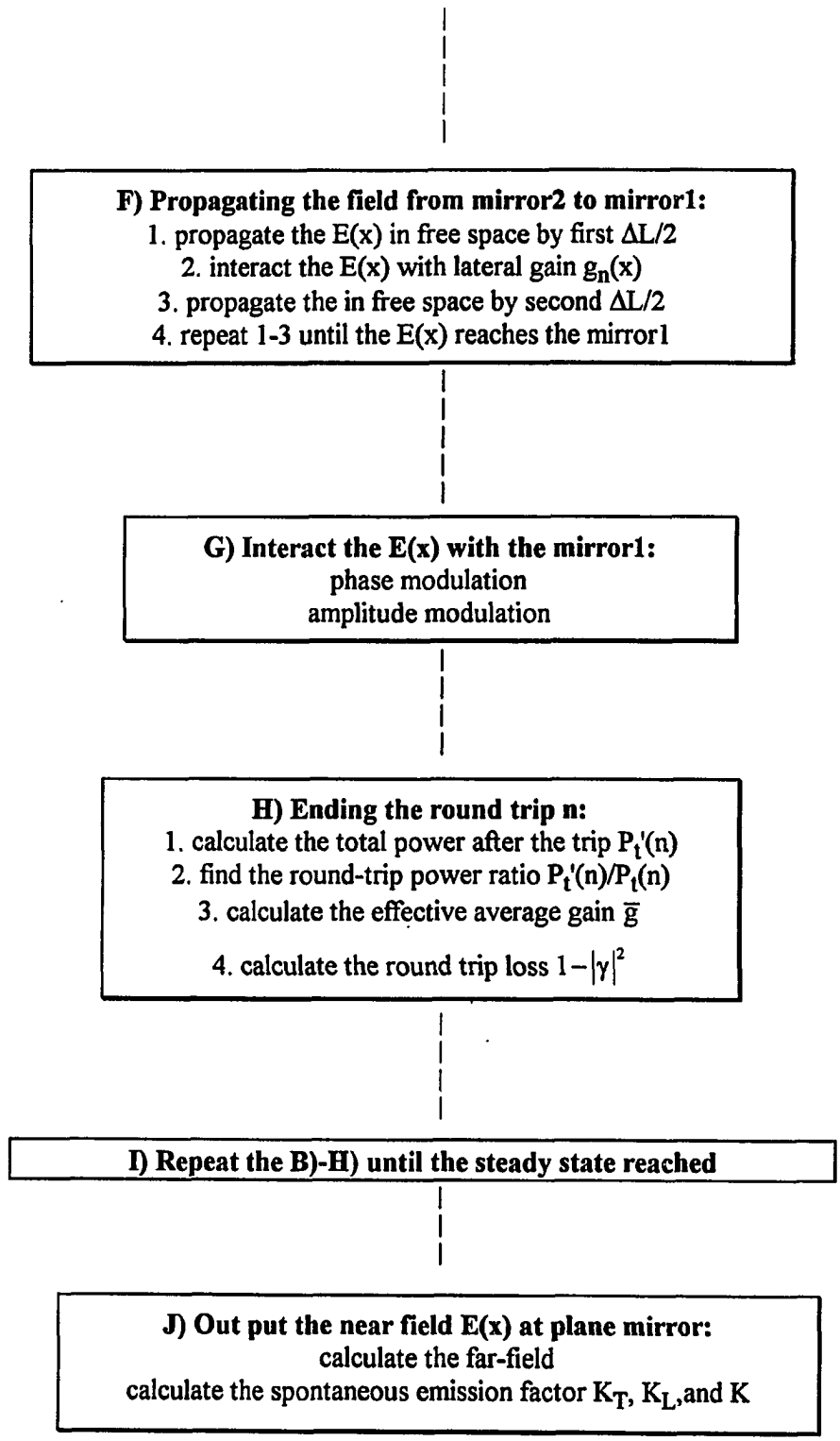

```
c **********************************
c program code of modal calculation for an
c unstable-resonator semiconductor laser
c **********************************

      parameter(NN=4096,pi=3.14159265359)
      real data(2*NN),s(NN),x(NN)
      real pump(NN)
      real power1,power2,pr,aui,ui,ur
      real xt,xmin,xmax,stpx,stps,stpz,rad1
      real ff,k0,wl,Lz,ui0,uibl,uisl,wx,dl,rr,fgs,fls
      integer Nz,i0,i1,i2,i3,time1,time2,Ntrip,Nout,inifst
      complex u(NN),j
      common k0,wl
      integer*2 ihr,imin,isec,i100th

      open (1,file='usl.sda')
      read (1,204) ur,ui0,uibl,uisl
      read (1,201) Nz,Ntrip,Nout,inifst
      read (1,202) wl,lz
      read (1,203) wx,dl,rad1
      read (1,202) xmax,xmin
      read (1,203) fgs,fls,zi

200   format(/8x,f8.7)
201   format(/8x,4(I8))
202   format(/8x,2(f8.7))
203   format(/8x,3(f8.7))
204   format(/8x,4(f8.7))

      write(*,*) ur,ui0,uibl,uisl
      write(*,*) Nz,Ntrip,Nout,inifst
      write(*,*) wl,lz
      write(*,*) wx,dl,rad1
      write(*,*) xmax,xmin
      write(*,*) fgs,fls,zi
      close(1)

      j=(0.,1.)
      k0=2.*pi/wl
      stpx=(xmax-xmin)/float(NN-1)
      stps=1./(stpx*float(NN))
      stpz=Lz/float(Nz)
      M=NN/2
```

```
c ------------------------------------------------------------
c assign NN grid points in space and frequency domain
c ------------------------------------------------------------

        do 1,i=1,M
          if(i.eq.1)then
           xt=xmin
          else
           xt=xt+stpx
          endif
          x(i)=xt
          x(NN-i+1)=-xt
1     continue

        do 2,i=1,M+1
          s(i)=(i-1)*stps
          if(i.ge.2)then
          s(NN-i+2)=s(i)
          endif
2     continue

c -----------------------------------
c assign NN points of complex index u(NN)
c -----------------------------------

53     format(2(e16.7))
       call index(x,u,ui0,wx,dl,NN)

       open(1,file='pump.dat')
        do 6,i=1,NN
       pump(i)=aimag(u(i))
      write(1,*) i,pump(i)
6     continue
      close(1)

c -----------------------------------
c assign initial field in data(NN)
c -----------------------------------

        call inifield(zi,x,data,NN)
```

```
c ------------------------------------------------------------
c cicling the field in z direction by N  times.  after
c each round trip, find the power-ratio before and after
c the round trip;  and the round trip loss was calculated
c based on the power ratio.
c ------------------------------------------------------------

        call GETTIM (ihr,imin,isec,i100th)
        time1=ihr*60+imin+isec/60
        pr=0.
        i0=0

c ----------------------------------
c find the total power before the trip
c----------------------------------
        power1=0.
        power2=0.
        do 40, i=1,NN
        power1=power1+(data(2*i)**2+data(2*i-1)**2)
40      continue

c----------------------------------
c start the circling
c----------------------------------

        do 45,i0=1,Ntrip

        write(*,44) ' start trip',i0
44      format(a11,i6)

c---------------------------------
c modify the gian
c---------------------------------
          do 31,i=1,NN
          ff=data(2*i-1)*data(2*i-1)+data(2*i)*data(2*i)
          ui=( (pump(i)-uibl)/(1+ff/fgs) ) - (uisl/(1+ff/fls))
          u(i)=ur+j*ui
31        continue

          do 41 i1=1,Nz
          call stepz(data,u,s,NN,stpz)
41        continue
```

```
        call mirror1(x,data,NN,rad1)

        do 42 i2=1,Nz
        call stepz(data,u,s,NN,stpz)
42      continue

        call mirror2(data,NN)

c---------------------------------------
c find the total power after the trip
c---------------------------------------
        power2=0.
        aui=0.
        do 43, i3=1,NN
        ff=data(2*i3)**2+data(2*i3-1)**2
        power2=power2+ff
        aui=aui+aimag(u(i3))*ff
43      continue

c---------------------------
c find the round trip loss
c---------------------------
        pr=power2/power1
        power1=power2
        aui=aui/power2
        rr=pr*exp(-4.*lz*k0*aui)
        ff=data(NN)**2+data(NN-1)**2
        write(*,*) 'avgain,  loss,  pratio,  center power '
        write(*,*) aui,1-rr,pr,ff

45      continue
c-------------------------------
c end of circling of the field
c -------------------------------

        call kfactor(stpx,data,rr,NN,temp,2)
        close(2)
        call GETTIM (ihr,imin,isec,i100th)
        time2=ihr*60+imin+isec/60
        write(*,101) ' total time =  ', time2-time1

101     format(A15,I5)
        end
```

```
c sub1
c ****************************************************
c give value NN points of x(NN), return initial field in data(2*NN)
c ****************************************************

      subroutine inifield(zi,x,data,NN)
      parameter(pi=3.14159265359)
      real k0,zi,sd,r1,r2,r
      complex field1,field2,field,j
      dimension x(NN),data(2*NN)
      common k0

      j=(0.,1.)
      M=NN/2
      sd=2000.
      do 10, i=1,M
        r1=sqrt((x(i)+sd)**2 + zi*zi)
        r2=sqrt((x(i)-sd)**2 + zi*zi)
        r=sqrt(x(i)**2 + zi*zi)
        field1=(1./r1)*exp(-j*k0*r1)
        field2=(1./r2)*exp(-j*k0*r2)
        field=(1./r)*exp(-j*k0*r)
c     field=field1+field2+field
        data(2*i-1)=real(field)
        data(2*(NN-i)+1)=data(2*i-1)
        data(2*i)=aimag(field)
        data(2*(NN-i)+2)=data(2*i)
10    continue

      return
      end

c sub2
c ************************************************************
c give value of NN points x(NN), return NN points of complex index,u(NN)
c ************************************************************
      subroutine index(x,u,ui0,wx,dl,NN)
      real x(NN),indexr,indexi0,indexi1
      real hw,dl,ui0,wx
      complex u(NN),j

      hw=wx/2.
      j=(0.,1.)
```

```
      do 10 i=1,NN
      u(i)=indexr(x(i)) + j*indexi0(x(i),hw,dl,ui0)
10    continue

      return
      end

      real function indexr(xt)
      real xt
      indexr=1.8
      return
      end

      real function indexi0(xt,hw,dl,ui0)
      real xt,a,hw,dl,ui0,ss
      a=log(1000.)/dl
      ss=a*(abs(xt)-hw)
      if(ss.gt.3000.)then
      indexi0=0.
      else
      indexi0=ui0/(exp(ss)+1.)
      endif
      return
      end

      real function indexi1(xt,wx,ui0)
      real xt,wx,ui0,ss
      a=4.*( log( (ui0)/(0.5*ui0) ) ) /(wx*wx)
      ss=a*xt*xt
      if(ss.gt.3000.)then
      indexi1=0.
      else
      indexi1=((ui0)*exp(-a*xt*xt))
      endif

      return
      end
```

```
c sub3
c
**********************************************************************
c advance the wave data(NN)  in z direction by stpz.  the field is first resolved
c into paraxial plane wave components by calling  subroutine  FOUR1(). The
c paraxial wave components are then propagated in free space by distance stpz/2.
c Then new components are used to reconstruct the new field at z+stpz/2 by calling
c FOUR1() for inverse transfer again. The field at z+stpz/2 is then mutiplied by a gain
c sheet and the resulting  field is propagated with rest  stpz/2 trip in free space by
c calling  FOUR1() twice again.
c **************************************************************

      subroutine stepz(data,u,s,NN,stpz)
      parameter(pi=3.14159265359)
      real hstpz,stpz,k0,wl,dk,ur
      complex u(NN),field,j
      real data(2*NN),s(NN)
      common k0,wl

      hstpz=stpz/2.
      j=(0.,1.)

c ---------------------------------------------
c proceed field in free space from z to z+stpz/2
c ---------------------------------------------
      call four1(data,NN,1)

      do 10 i=1,NN
        ur=1./real(u(i))
        field=data(2*i-1)+j*data(2*i)
        dk=pi*wl*s(i)*s(i)*ur*(1.+wl*wl*ur*ur*s(i)*s(i)/4.)
        field=field*exp( j*hstpz*dk )
        data(2*i-1)=real(field)
        data(2*i)=aimag(field)
10    continue

      call four1(data,NN,-1)
c ---------------------------------------------
c mutiply gain sheet to the field at z+stpz/2
c ---------------------------------------------
      do 20 i=1,NN
        field=data(2*i-1)+j*data(2*i)
        field=(field/float(NN))*exp(-j*stpz*k0*u(i))
        data(2*i-1)=real(field)
```

```
          data(2*i)=aimag(field)
20      continue
c ---------------------------------------------------
c proceed the field in free space from z+stpz/2 to z+stpz
c ---------------------------------------------------
        call four1(data,NN,1)

        do 30 i=1,NN
          ur=1./real(u(i))
          field=data(2*i-1)+j*data(2*i)
          dk=pi*wl*s(i)*s(i)*ur*(1.+wl*wl*s(i)*s(i)*ur*ur/4.)
          field=field*exp( j*hstpz*dk )
          data(2*i-1)=real(field)
          data(2*i)=aimag(field)
30      continue

        call four1(data,NN,-1)

        do 40 i=1,NN
          data(2*i-1)=data(2*i-1)/float(NN)
          data(2*i)=data(2*i)/float(NN)
40      continue

        return
        end

c sub4
c ************************************************
c give NN points of complex field u(i) at x(i), the program reflects
c the field on  a spherical mirror with reflectivity rf1 and radious
c of curvture R1.
c ************************************************

        subroutine mirror1(x,data,NN,rad1)
        complex field,j
        real x(NN),data(2*NN)
        real k0,rf1,ur0,phase,rad1
        common k0

        j=(0.,1.)
        rf1=0.55
        ur0=3.6

        do 10 i=1,NN
          field=rf1*(data(2*i-1)+j*data(2*i))
```

```
          phase=k0*ur0*x(i)*x(i)/rad1
          field=field*exp(-j*phase)
          data(2*i-1)=real(field)
          data(2*i)=aimag(field)
10      continue
        return
        end

        subroutine mirror2(data,NN)
        real data(2*NN)
        real rf2

        rf2=0.55

        do 10 i=1,NN
          data(2*i-1)=rf2*data(2*i-1)
          data(2*i)=rf2*data(2*i)
10      continue

        return
        end

c sub5
c ***********************************************
c tranfer near field data into farfield and write in file 'ff.dat'
c ***********************************************

        subroutine farfield(x,stpx,data,NN,nfc)
        parameter(pi=3.14159265359)
        real x(NN),data(2*NN)
        real fc,agmax,agmin,stpag,stpx,k0
        complex ffield,j,field
        common k0

        j=(0.,1.)
        fc=pi/180.
        Nag=800
        agmax=40.*fc
        agmin=-40.*fc
        stpag=(agmax-agmin)/Nag

        ag=agmin
        do 10 i0=1,Nag

        ag=ag+stpag
```

```
      ffield=(0.,0.)
      do 20 i=1,NN
      field=data(2*i-1)+j*data(2*i)
      ffield=ffield+field*stpx*exp( j*k0*x(i)*sin(ag) )
20    continue

      ff=(real(ffield)*real(ffield)+aimag(ffield)*aimag(ffield))
      ff=cos(ag)*cos(ag)*ff/(NN*NN)
      write(nfc,21) ag/fc, ff

10    continue
21    format(2(e16.7))

      return
      end

c sub 6
c ***********************************************
c calculate the enhancement factor of spontaneous emission
c factor K_l, K_t, and K based on near field and round-trip loss
c ***********************************************
      subroutine kfactor(stpx,data,rr,NN,temp,nfk)
      real data(2*NN),rr,temp
      real stpx,pft,pfl,sum1
      complex sum2

      sum1=0.
      sum2=0.
      do 10, i=1,NN
      sum1=sum1 + stpx*( data(2*i-1)**2 + data(2*i)**2 )
      sum2=sum2 + stpx*( cmplx(data(2*i-1),data(2*i)) )**2
10    continue

      pft=sum1*sum1/(real(sum2)**2 + aimag(sum2)**2)
      pfl=(1./rr)*( (1.-rr)/(log(1./rr)) )**2
      print*, 'M=   ', (0.55*0.55)/rr
      print*, 'rr=  ',1-rr
      print*, 'pft= ',pft
      print*, 'pfl= ',pfl
      print*, 'pflt= ', pft*pfl
      write(nfk,11) temp,rr,pft,pfl
11    format(4(e16.7))
      return
      end
```

```
c sub 7
c ****************************************
c One dimensional complex Fast Fourier Transform
c ****************************************
      SUBROUTINE FOUR1(DATA,NN,ISIGN)
      REAL*8 WR,WI,WPR,WPI,WTEMP,THETA
      DIMENSION DATA(*)
      N=2*NN
      J=1

      DO 11 I=1,N,2
        IF(J.GT.I)THEN
          TEMPR=DATA(J)
          TEMPI=DATA(J+1)
          DATA(J)=DATA(I)
          DATA(J+1)=DATA(I+1)
          DATA(I)=TEMPR
          DATA(I+1)=TEMPI
        ENDIF
        M=N/2
1       IF ((M.GE.2).AND.(J.GT.M)) THEN
          J=J-M
          M=M/2
        GO TO 1
        ENDIF
        J=J+M
11    CONTINUE
      MMAX=2
2     IF (N.GT.MMAX) THEN
        ISTEP=2*MMAX
        THETA=6.28318530717959D0/(ISIGN*MMAX)
        WPR=-2.D0*DSIN(0.5D0*THETA)**2
        WPI=DSIN(THETA)
        WR=1.D0
        WI=0.D0

        DO 13 M=1,MMAX,2
          DO 12 I=M,N,ISTEP
            J=I+MMAX
            TEMPR=SNGL(WR)*DATA(J)-SNGL(WI)*DATA(J+1)
            TEMPI=SNGL(WR)*DATA(J+1)+SNGL(WI)*DATA(J)
            DATA(J)=DATA(I)-TEMPR
            DATA(J+1)=DATA(I+1)-TEMPI
            DATA(I)=DATA(I)+TEMPR
            DATA(I+1)=DATA(I+1)+TEMPI
```

```
12      CONTINUE
          WTEMP=WR
          WR=WR*WPR-WI*WPI+WR
          WI=WI*WPR+WTEMP*WPI+WI
13    CONTINUE
        MMAX=ISTEP
    GO TO 2
    ENDIF
    RETURN
    END
```

References

1. A. P. Bogatov, P. G. Eliseev, M. A. Man'ko, G. T. Mikaelyan, and Yu. M. Popov, Sov. J. Quantum Electron., vol. 10. p. 620, (1980)
2. R. R. Craig, L. W. Casperson, O. M. Stafsudd, J. J. Yang, G. Evans, and R. Davidheiser, Electron. lett., vol. 21, p. 62, (1985)
3. R. lang, M. Mittelstein, A. Yariv, and J. Salzman, IEEE, Proceedings, Vol. 134, Pt. J, No. 1, p.69 and p. 96, (1987)
4. H. Wang, Y. Y. Liu, M. Mittelstein, T. R. Ehen, and A. Yariv, Electron Lett., vol. 23, no. 18, p. 949, (1987)
5. M. L. Tilton, G. C. Dente, A. H. Paxton, Proc. SPIE laser-diode Technol. Appl. II, vol. 1219, p. 423, (1990)
6. M. L. Tilton, G. C. Dente, A. H. Paxton, J. Cser, R. K. Defreez, C. E. Moeller and D. Depatie, IEEE J. Quantum Electron. QE-27, p. 2098, (1991)
7. K. Petermann, IEEE J. Quantum Electron., QE-15, p. 566, (1979)
8. A. Yariv and S. Margalit, IEEE J. Quantum Electron. QE-8, p.1831, (1982)
9. M. Newstein, IEEE J. Quantum Electron., QE-20, p.1270, (1984)
10. H. A. Haus and S. Kawakami, IEEE J. Qunaatum Electron. QE-21, p. 63, 1985
11. C. H. Henry, IEEE J. Lightwave Technol. LT-4, p. 288, (1986)
12 Jean-luc Doumont, Paul L. Mussche, and A. E. Siegman, IEEE, J. Quantum Electron, QE-25, p1960, (1989)
13. A. E. Siegman, Phys. Rev. A 39, p. 1252 and 1264, (1989)
14. W. A. Hamel and J. P. Woerdman, Phys. Rev. A40, p. 2785, (1989)
15. W. A. Hamel and J. P. Woerdman, Phys. Rev. A40, p. 1506, (1990)

16. A. E. Siegman, Lasers, 3rd Edition, University Science Books, Mill Valley, CA, (1986)

17. Yasuharu Suematsu, Shigeyuke Akiba, and Tchanchee Hong, IEEE, J. Quantum Electron, QE-13, p.596, (1977)

18. A. G. Fox and T. Li, IEEE J. Quantum Electron, QE-4, p. 460, (1968)

19. G. P. Agraw, N. K. Dutta Long wave length semiconductor lasers 1st Edition, Van Nostrand Reinhold, New York, NY(1986)

20. A. G. Fox and T. Li, Bell. Sys. Tech. J. 40, p. 453, (1961)

21. M. Lax, J. H. Battech, G. P. Agrawal, J. Appl. Physics. 52(1), p. 109, (1981)

22. G. P. Agrawal, W. B. Joyce, R. W. Dixon, and M. Lax, Appl. Phys. Lett., 43(1), p. 11, (1983)

23 G. Yao, Y. C. Chen, C. M. Harding, S. M. Sherrik, R. J. Dalby, R. G. Waters, and C. Largent, Optics Letters, Vol. 17, No. 17, p. 1207, (1992)

24. C. H. Henry, IEEE J. Quantum Electron. QE-18, p. 259 (1982)